# An integrated organoid omics map extends modeling potential of kidney disease

**Moritz Lassé**
III. Department of Medicine, University Medical Center Hamburg-Eppendorf (UKE), Hamburg, Germany
**Sean Eddy**
University of Michigan
**Jamal El Saghir**
Department of Internal Medicine, Division of Nephrology, University of Michigan Medical School, Ann Arbor, USA
**Matthew Fischer**
Department of Internal Medicine, Division of Nephrology, University of Michigan Medical School, Ann Arbor, USA
**Arvid Hutzfeldt**
University Medical Center Hamburg-Eppendorf https://orcid.org/0000-0001-5993-1991
**Celine Berthier**
University of Michigan
**Léna Bonin**
Department of Biomedicine, Aarhus University, Aarhus, Denmark
**Bernhard Dumoulin**
University Medical Center Hamburg-Eppendorf
**Rajasree Menon**
Department of Computational Medicine and Bioinformatics, University of Michigan Medical School, Ann Arbor, Michigan, USA
**Virginia Vega-Warner**
University of Michigan
**Felix Eichinger**
Department of Internal Medicine, Division of Nephrology, University of Michigan Medical School, Ann Arbor, USA
**Fadhl Alakwaa**
University of Michigan,
**Damian Fermin**
University of Michigan–Ann Arbor
**Phillip McCown**
Department of Internal Medicine, Division of Nephrology, University of Michigan Medical School, Ann Arbor, USA

**Bradley Godfrey**
Department of Internal Medicine, Division of Nephrology, University of Michigan Medical School, Ann Arbor, USA
**Paul Brandts**
III. Department of Medicine, University Medical Center Hamburg-Eppendorf (UKE), Hamburg, Germany https://orcid.org/0000-0002-0649-3569
**Wenjen Ju**
Department of Internal Medicine, Division of Nephrology, University of Michigan Medical School, Ann Arbor, USA
**Linda Reinhard**
University Medical Center Hamburg-Eppendorf https://orcid.org/0000-0001-9786-9922
**Elion Hoxha**
III Medical Clinic and Polyclinic, Nephrology
**Florian Grahammer**
III. Department of Medicine, University Medical Center Hamburg-Eppendorf, Hamburg, Germany
**Maja Lindenmeyer**
III. Department of Medicine, University Medical Center Hamburg-Eppendorf, Hamburg, Germany
**Tobias Huber**
Albert-Ludwigs-Universität Freiburg https://orcid.org/0000-0001-7175-5062
**Hartmut Schlüter**
University Medical Center Hamburg-Eppendorf https://orcid.org/0000-0002-9358-7036
**Steffen Thiel**
Aarhus University https://orcid.org/0000-0002-4817-155X
**Laura Mariani**
Department of Internal Medicine, Division of Nephrology, University of Michigan Medical School, Ann Arbor, USA
**Matthias Kretzler**
University of Michigan Ann Arbor https://orcid.org/0000-0003-4064-0582
**Fatih Demir**
Aarhus University https://orcid.org/0000-0002-5744-0205
**Jennifer Harder** ( jlharder@med.umich.edu )
Department of Internal Medicine, Division of Nephrology, University of Michigan Medical School, Ann Arbor, USA
**Markus Rinschen**
III Department of Medicine University Medical Center Hamburg-Eppendorf, 20246 Hamburg, Germany

---

**Article**

**Keywords:**

**Posted Date:** October 5th, 2022

**DOI:** https://doi.org/10.21203/rs.3.rs-2109564/v1



**Version of Record:** A version of this preprint was published at Nature Communications on August 14th, 2023. See the published version at https://doi.org/10.1038/s41467-023-39740-7.

# Abstract

Kidney organoids are a promising model to study kidney disease, but use is constrained by limited knowledge of their functional protein expression profile. We aimed to define the organoid proteome and transcriptome trajectories over culture duration and upon exposure to TNFα, a cytokine stressor. Older organoids increased deposition of extracellular matrix but decreased expression of glomerular proteins. Single cell transcriptome integration revealed that most proteome changes localized to podocytes, tubular and stromal cells. TNFα-treatment of organoids effected 320 differentially expressed proteins, including cytokines and complement components. Transcript expression of these 320 proteins was significantly higher in individuals with poorer clinical outcomes in proteinuric kidney disease. Key TNFα-associated protein (C3 and VCAM1) expression was increased in both human tubular and organoid kidney cell populations, highlighting the potential for organoids to advance biomarker development. By integrating kidney organoid omic layers, incorporating a disease-relevant cytokine stressor and comparing to human data, we provide crucial evidence of functional relevance of the kidney organoid model to human kidney disease.


# Introduction

Organoids are emerging as an increasingly important model system to understand development and disease. Kidney organoids have been used to model kidney cancer, glomerular diseases and podocytopathies, basement membrane development and disease, polycystic kidney disease (PKD), and renal tubular epithelia ciliopathies [1–7]. Additionally, organoids have been proposed as a promising screening tool for therapeutics, as well as a model of virus infection and organ cryopreservation, especially when combined with high throughput methods [1,4,8–12]. Organoids are employed to improve our understanding of genetic kidney diseases and are used as models to interrogate kidney development and molecular mechanisms [13–16]. When generated from human pluripotent stem cells, kidney organoids recapitulate elements of human kidney disease which are lacking in animal models and traditional 2D tissue culture models [17].

Significant effort by us and others [1,18–22] has defined single cell transcriptional profiles of kidney organoids. However, transcripts do not necessarily correspond to protein abundance, especially in very dynamic systems [23]. In addition, several dimensions of the proteome are not amenable to transcript-based analysis, including the secretome, which is the entirety of secreted proteins. Until now, the proteome of human kidney organoids has been insufficiently characterized; it is still unclear how their proteome changes during differentiation, and whether the protein composition of kidney organoids is sufficient to model more complex disease processes such as that seen, for instance, in inflammatory tissue responses. Through recent advances in large-scale proteome acquisition technologies, novel perspectives on tissue biology in kidney disease have been gained. We can harness these novel technologies and insights to both define the proteome of kidney organoids more fully, and to further evaluate their relevance to human kidney disease.

Using transcriptional profiling, we recently demonstrated that proinflammatory molecular signals, likely orchestrated through cytokines such as TNFα, were observed in kidney tissue from individuals with poor clinical outcomes in proteinuric kidney disease. For many kidney diseases, individualization of therapy is challenged by diverse underlying pathomechanisms[24]. Thus, a more exhaustive proteomics analysis of kidney organoids would further enhance our understanding of proinflammatory events associated with these putative inflammatory drivers of disease.

The data we present here provide critical foundational knowledge of kidney organoids as a model system of human kidney disease. First, we describe how the organoid proteome and transcriptome evolve as a function of culture duration and identify organoid cell types in which protein expression changes. Then we compare the expression of podocyte-specific proteins in organoids to the expression observed in native glomeruli and cultured podocyte cells. Finally, we demonstrate that organoids react to TNFα with a global inflammatory response similar to the molecular changes associated with poor outcomes for individuals with FSGS/MCD. These protein signatures can directly add to an individual's disease stratification and suggest additional disease-relevant biomarkers. Together, this characterization of kidney organoids based on integration of proteome and transcriptome along with the demonstration of innate immune responses in organoid cell types expands the scope of organoids as a discovery platform for the cellular biology of kidney disease and potential therapeutics. Moreover, we provide a rich resource to the research community to promote ongoing kidney disease modeling, biomarker discovery and therapeutic screening.

# Results

### Analysis of the kidney organoid trajectory.

Building on work generated by us and others showing that kidney organoids around 3 weeks in culture display glomerular differentiation characteristic of developing human kidneys [18,22] we performed proteomic and transcriptional profiling [1,25] on organoids cultured between 21 and 29 days. Proteomic analysis was performed on 20 organoid spheroids at four time points during the differentiation trajectory. In total, more than 6,700 proteins were identified (*Suppl Table 1*). Of these identified proteins, 5,403 proteins could be quantified across samples. Principal component analysis revealed separation of organoid proteomes from days 21 to 25 to 27 to 29 (*Suppl Fig. 1A*). We performed differential analysis of these 5,403 proteins between days 29 and 21 of differentiation and detected 350 proteins that were significantly upregulated, and 428 proteins which were significantly downregulated (FDR < 0.05 *Fig. 1A and Suppl Table 2*). Key podocyte markers, such as nephrin (*NPHS1*) and synaptopodin (*SYNPO*), indicating glomerular differentiation, decreased with time in culture indicating a relative loss of podocytes or a relative increase of other cell populations (*Fig. 1A*). Meanwhile, structural proteins such as smooth muscle actin (*ACTA2*) and key regulatory differentiation proteins such as Platelet-derived growth factor receptor alpha (*PDGFRA*) were increased (*Fig. 1A*), suggesting increased production of extracellular matrix. These observations were validated by immunofluorescence (*Fig. 1B*). To further visualize culture duration-dependent trajectories, we normalized protein expression data and performed row-wise

hierarchical clustering (*Fig. 1C*) followed by GO-term annotation of the respective proteins and clusters. Five clusters (of size > 25 proteins) were distinguished (*Fig. 1D*). The data confirmed the patterns of an increase in extracellular matrix proteins (*Fig. 1D, clusters 1 and 3*) and a decrease in glomerular development proteins (*Fig. 1D, cluster 5*) with culture duration.

### Organoid proteome-transcriptome integration uncovers cellular origins of proteins.

To further assess gene expression dynamics in organoids relative to duration in culture, we integrated proteomic with bulk RNA sequencing data of corresponding organoid spheroids at days 21, 25, and 29 (*Fig. 2A*). Although measured quantities of protein and RNA (*Suppl Table 3*) did not correlate strongly (R = 0.27, 0.24, 0.24 on days 21, 25, 29 respectively), the relationship between protein and RNA expression remained consistent across the days in culture as indicated by 2D keyword enrichment of basic functional terms, including 'Differentiation', 'Glycolysis', 'Mitochondrion', 'TCA-cycle' and 'Proteinbiosynthesis' (*Fig. 2A, 2B*). To understand which cell types contribute to the proteome, we sought to define the cellular composition of organoids by employing single cell RNA sequencing (scRNA-seq). Integrated clustering of organoid-specific single cell datasets conducted within our study revealed 14 different organoid cell types, 60% of cells identified as target kidney cell types (*Figs. 2C and 4A, Suppl Table 4*). Each of these cell types contributed to the data observed in bulk proteomic and bulk RNA sequencing analysis. To define which cell types may undergo the most dramatic changes in cellular organization during cell culture on the protein level, we mapped transcript markers of these 14 cell clusters to the proteomics dataset. This approach is feasible as scRNA-seq and proteomics markers are largely consistent [26]. This analysis suggested that the largest proteome changes occur in the stromal cell population as indicated by over-expression of proteins related to stromal markers on day 29 compared with day 21 (*Fig. 2D*). Of the kidney-specific cell types, early glomerular epithelial cells and maturing podocytes seem to become less represented with duration in culture as indicated by under-expression of associated markers at the later timepoint. This is consistent with our earlier findings showing diminished podocyte and increased stromal cell specific protein expression (*Figs. 1B/C/D and 2E*). To understand which proteins were most associated with these observed changes, we clustered protein and RNA expression data of the top 30 differentially expressed proteins by cell type marker. The pattern of expression of these 30 proteins corresponded to observed changes in both protein and RNA levels. The majority (≥ 90%) of the top 30 differentially expressed proteins decreased over time on both protein and RNA levels in the glomerular epithelium, podocytes and proximal tubules (*Fig. 2E*). This contrasted with the stroma, where the top 30 differentially expressed proteins increased over time. Together, these results suggest a loss of expression of kidney-specific proteins in older organoids, highlighting the need to identify optimal culture time point for expression of proteins of interest when modeling disease.

### Comparison of organoid proteome organization with mature human tissue.

We next sought to determine how proteomes of organoids, human kidney and immortalized podocytes overlapped. First, proteomes of organoids and microdissected adult single human tubules and single glomeruli were compared using a technology previously developed [27] (*Fig. 3A*). We achieved a six-fold

deeper proteome coverage for organoids (n = 6,703 proteins) compared to single glomeruli (n = 1,002 proteins) or tubule native tissue extracts (n = 1,730 proteins). Notably, the proteome from organoids covered 88% of the proteome of single glomeruli and 84% of the proteome of single tubules. GO-term over-representation analysis (*Fig. 3B)* indicated that the organoid proteome comprised of enriched gene sets corresponding to receptor-mediated signaling and 'Extracellular Matrix (ECM)' components, while immortalized podocytes (*Fig. 3C*) demonstrated isolated proteins related to cell cycle and catabolic processes. Furthermore, the proteome copy numbers of key podocyte proteins in organoids were similarly distributed to those observed in mature native human and mouse podocytes, as compared to the relatively low numbers observed in immortalized podocytes (*Fig. 3D*). Some GO-terms were less represented in the organoids compared to human kidney components suggesting limitations to their modeling ability, including "glomerular vasculature" and "collagen type IV" and as well as "brush border", "glucose:sodium- and urate-transport" representing proteins involved in classical proximal tubule function and solute transport. Together, these results indicate that kidney organoids faithfully represent the majority of proteins expressed in human kidneys, including key podocyte proteins, and are superior in this respect to immortalized podocytes.

**Organoids respond to TNFα with activation of proinflammatory proteins.**

In a recent study, we showed that TNFα-treated kidney organoids expressed key transcripts and proteins associated with TNFα activation and poor clinical outcomes in FSGS and MCD [24]. The expressed molecules included the chemokine ligand 2 (also known as monocyte chemoattractant protein 1, MCP-1, encoded by *CCL2*) and tissue inhibitor of metalloproteinases 1 (*TIMP1*). Building on insights of proteome organization of our organoid model (*Fig. 1–3*), we aimed to further define TNFα activation in kidney organoids. Though TNFα receptors TNFRSF1A and TNFRSF1B (encoded by *TNFRSF1A* and *TNFRSF1B*, respectively [28]) were not detected in organoids by proteomics, expression was detected by scRNA-seq analysis, with *TNFRSF1A* expression far exceeding that of *TNFRSF1B.* Further, immunofluorescence indicated strong expression of TNFRSF1A in N-cadherin (*CHD1*) + proximal tubular cells (*Fig. 4A/B, Suppl Table 1*). Given these findings, organoids were treated with TNFα to study their proteomic response (*Fig. 4C, Suppl Table 5*). After 24h of TNFα stimulation, organoid cell lysates demonstrated a significant increase in Vascular cell adhesion protein 1 (VCAM1) concentration (FDR $p < 0.1$), which persisted to 48h. After 48h of TNFα treatment, 145 proteins were increased, and 157 proteins were decreased (FDR < 0.1) in the organoid proteome. Increased proteins included VCAM1, intercellular adhesion molecule 1 (ICAM1), Nuclear factor NF-kappa-B (NFkB2) and integrin alpha-3 (ITGA3). Protein markers of early glomerular epithelial cells were most altered with TNFα treatment compared with protein markers of other cell types (*Fig. 4D*). Stromal cells yielded the lowest response with TNFα treatment.

To investigate possible signaling systems deployed by organoids upon TNFα exposure, we also analyzed the proteins secreted from organoid cells into the overlying culture medium, the so-called secretome. To define the medium at baseline, analysis without exposure to organoids was carried out and revealed a total of 23 proteins not commonly observed as contaminants as part of the MaxQuant contaminant database [29] (*Suppl Table 6*). The organoids secreted an additional ~ 120 detectable proteins on average,

a number marginally increased with addition of TNFα (*Suppl Fig. 1B*). Differentially expressed and secreted proteins included cell adhesion proteins but also regulators of apoptosis and cell death (SFRP2 and IGFBP7) and extracellular matrix proteins (LAMB1, HSPG2, PTX3 and BGN). Intriguingly, we found that TNFα treatment increased the secretion of the cytokine CXCL10 as well as several complement components (C1s, C3, C1q). Increased complement and cytokine expression was already visible after 24h (*Fig. 4E, Suppl Table 7*), and C1R and C1S expression was detected after 48h of TNFα exposure. Importantly, these changes were robustly reproducible, as demonstrated by focused analysis of CXCL10 transcript as well as intracellular plus secreted protein levels following 24h and 48h of TNFα exposure (*Fig. 4F*). These analyses of the secretome demonstrate that kidney organoids (devoid of immune cell types) are capable of secreting proteins involved in cytokine signaling. This is absent in cultured podocytes treated with the same concentration of TNFα (*Suppl Tables 8 and 9, Suppl Fig. 2A-H*), indicating that the protein expression profile of TNFα-treated organoids had a more complex biological response (particularly noticeable in the secretome) compared with the human cultured podocyte model.

**Proteome alterations in TNFα-induced organoids help stratify diseased human kidney tissue.**

To determine the translatability of the TNFα-driven changes observed in organoid proteomes to human kidney disease, we compared these changes to our previously characterized gene signature of TNF activation, encompassing 272 genes. Summary gene expression of this gene set identified a subgroup of individuals with MCD or FSGS who had poorer outcomes within the NEPTUNE study [24] (*Fig. 5A)*. We asked whether kidney organoids, containing kidney cells but no immune cells, could further focus this tissue-based signature to reveal kidney cell-specific pathomechanisms associated with poor outcome. To explore this idea, a new 320 gene product signature was derived from all differentially expressed proteins identified in TNFα-treated organoids (*Fig. 4C,D, Suppl Table 10*). Ten genes were shared by the two gene signatures as shown in *Fig. 5B* and Table 1. These included CXCL10 and cytokine response genes ICAM1, VCAM1, MAP4K4, PTX3 as well as complement factor C3. Most are known to be linked with TNFα-associated inflammation, and diverse range of kidney diseases summarized in Table 1. Half of the ten proteins were identified in the secretome (gene names in red and blue in *Fig. 5B*), prioritizing potential biomarkers of TNFα activity. Importantly, pathway analysis of genes from both signatures independently and in combination (total 582 genes) revealed multiple instances of TNF network activity (*Suppl. Tables 11 and 12*). However, the organoid-based gene signature revealed more about intracellular functions (amino acid and derivative metabolism, cellular response to stress, glycolysis, ATP synthesis), while the tissue based-signature encompassed more extracellular cytokine and immune system signaling. This suggests that the organoid-based signature is focused on gene activity at a more cell-based level as opposed to the complex milieu captured by the tissue-based signature. Each signature alone identified different aspects of gene connectivity based on literature-based network analysis (*Supp Fig. 3A*). This illustrates that complementary information can, indeed, be gleaned from adding the organoid model system to understand pathomechanisms of kidney disease. Performing analogous literature-based network analysis using all combined 582 genes and focused around the ten common proteins shows the unified interplay of these networks (*Fig. 5C*).

Table 1
Common genes between previously reported TNFα transcriptomic signature and TNFα-regulated proteins and their described function in kidney disease.

| Gene | | |
|---|---|---|
| BGN | A soluble proteoglycan associated with inflammatory kidney diseases; involved in modulating inflammatory signaling through Toll-like receptors thought to originate from activated macrophages; tissue based biglycan has been detected in crescentic GN; DKD and LCDD and amyloidosis. | 60–62 |
| HSP90B1 | Part of a group of ER stress response proteins involved in immunoregulation; affects processing and transport of secreted proteins; a polymorphism of HSP90B1 has been associated with glucorticoid response in individuals with SLE | 63,64 |
| CXCL10 | Increased in diverse kidney diseases: MesPGN, AKI, LN, DKD; expressed by resident kidney cells at low levels (note CXC3 receptor not expressed in our organoids sc or RNA-seq data) | 65,66 |
| ICAM1 | Expressed in kidney tubules in IgAN has been suggested as a marker of tubulointerstitial injury and predictor of disease progression | 67 |
| VCAM1 | expressed in PTECs in a variety of inflammatory kidney diseases, including diabetic kidney disease, urinary VCAM1 is suggested as biomarker of lupus nephritis activity | 68,69 |
| C3 | expression increases with TNFα stimulation in human glomerular endothelial cells | 70 |
| HSP90/GRP94 | ADPKD also p100 (NFKB2) and PKD affecting ciliary mechanosensation (Low et al.). | 71,72 |
| MAP4K4 | expressed in response to TNFα stimulation, reports of association with kidney disease are limited | 73 |
| OPTN | association with DKD, inhibition of cellular senescence through mitophagy via NLRP3 inflammasome inhibition in DKD. | 74,75 |
| PTX | expressed in response to inflammatory stimuli, and secreted into the plasma where levels inversely correlate with GFR and cardiovascular disease. Expressed in proximal tubular epithelial and mesangial cells as well as kidney fibroblasts | 76,77 |

When the organoid proteome-based 320 gene signature was applied to the same kidney-tissue transcriptome clusters as in *Fig. 5A*, significantly elevated summary transcript expression was observed in kidney tissue of individuals from cluster 3 of the cohort (*Fig. 5D*). In the original clinical study, cluster 3 associated with TNFα activation and encompassed the subgroup of individuals with poor FSGS/MCD related outcomes compared with individuals from clusters 1 and 2. The signature score was underwhelming for the disease group of 220 individuals as a whole (*Fig. 5D, far right bar*). Similarly, only a modest performance of the signature score was observed when the 320-gene signature was applied to tissue transcriptomic data from other groups of kidney disease types (*Suppl Fig. 3B, Suppl Table 10*). This underscores the critical need to continue efforts to identify subgroups of individuals in disease

cohorts who have different pathomechanisms of disease, and who may benefit from different targeted therapies.

When the 320-gene product signature was separated into signatures derived from either i) the secretome or ii) the cell lysate proteome alone (two proteins were present in both), each signature also could distinguish cluster 3 from clusters 1 and 2 on the transcriptional level in kidney tissue (*Fig. 5E*). Thus, both intracellular and secreted proteins expressed in TNFα-treated kidney organoids are relevant to individuals with poor outcome FSGS/MCD. Together, these data demonstrate that organoid cultures can both identify molecular pathobiology involved in disease phenotype and identify subgroups of individuals within a disease for whom this pathobiology is most relevant.

To further explore the disease relevance of the ten common genes in *Fig. 5B*, we returned to the NEPTUNE cohort, depicted in *Fig. 5A*. We interrogated snRNA-seq data [24] of a subset of ten participants for whom these data were available. This subset consisted of five participants with high TNFα activity score (cluster 3) and five participants with low TNFα activity score (cluster 1 or 2) (*Fig. 5F/G, Suppl Fig. 3D*). Even when transcript expression was combined across all cell types, most of the genes demonstrated differential expression in tissue from high versus low TNF activity (*Fig. 5F*) [30,31]. When the relatively small differential *CXCL10* expression in *Fig. 5F* was further examined on a cell type specific level (*Fig. 5G*), more pronounced differential expression was revealed in certain cell types in the high TNFα activity group (arrows), including immune cells as expected, as well as kidney cell types (podocytes and tubular cells). Similar cell-type specific expression findings could be seen in all ten genes in the human kidney samples as well as TNFα-treated organoids (*Suppl Fig. 3C/D respectively*). Taken together, these findings indicate that TNFα-treated kidney organoids capture key molecular mechanisms involved in poor outcome FSGS/MCD.

# TNFα-dependent molecules C3 and VCAM1 can stratify diseased kidney tissue

We further explored the ten common genes (shared between the 272-gene human tissue signature and the 320-gene organoid signature, *Fig. 5B*) as potential biomarkers of TNFa pathway activation, especially those discovered in the organoid secretome (strategy shown in *Fig. 6A*). Two genes (*C3* and *VCAM1*) were of particular interest given previous descriptions of their potential use as biomarkers in kidney disease (Table 1). Figure 6B shows the reproducibility of C3 and VCAM1 gene expression in TNFα-treated organoids at transcription and secreted protein levels, confirming our proteomic data (*Fig. 4C/E*). Single cell transcriptional profiling in *Fig. 6C* shows expression of *C3* and *VCAM1* in TNFα-treated organoid kidney cell types, while expression of C3 and VCAM1 for all organoid cell types with and without TNFα treatment is shown in *Suppl Figs. 4A/B and 3E*. Immunoblotting detected complement C3 in the media of the organoids only in the presence of TNFα (*Suppl Fig. 4C*). Together these results demonstrate that organoid kidney cell types express these genes upon TNFα stimulation and secrete resulting gene products.

To determine the relevance of these findings to FSGS/MCD, we returned to the NEPTUNE cohort (*Fig. 5A*). As shown in *Fig. 6D, C3* and *VCAM1* expression were both increased in the cluster of individuals with poorer outcomes in FSGS/MCD. We next posited that if these genes were potential biomarkers of TNFα activity in FSGS/MCD, expression should be higher in kidney cell types in individuals with high TNFα activity. Indeed, single nuclear transcriptional profiling of individuals (as in *Fig. 5E*) demonstrated higher expression of both *C3* and *VCAM1* in distal thin limb (DTL) tubular cell types (*Fig. 6E*), even when compared to immune cells. When these tubular cell types were isolated and expression separated by TNFα activity status, both *C3* and *VCAM1* were both significantly higher in cells from high TNFα status individuals.

# Discussion

Kidney organoids generated from human pluripotent stem cells (hPSC) have tremendous potential to advance our understanding of kidney development and disease [13,17,18,32]. However, thorough understanding of these complex structures as well as their relevance to human kidney disease is critical to their successful implementation as a model system. Here, we describe a comprehensive, deep analysis of proteins expressed and secreted by hPSC-kidney organoids and tie these findings to transcriptional changes that occur relative to organoid culture duration, fundamental knowledge needed to advance use of kidney organoids to model human disease. Crucially however, we extend our study beyond solely a description of expression of these gene products by also demonstrating the functionality and relevance of gene product networks in our organoid model system to TNFa-associated kidney disease.

We demonstrated how we could use our defined system to learn novel pathobiology relevant to TNFα associated kidney disease. Here, the absence of immune cells and vasculature allowed a reductionist approach to define the TNFα-induced proteome response relevant to intrinsic nephron cell population in FSGS/MCD. First, we built on previous tissue-based findings suggesting TNFα activity was associated with poor outcomes in FSGS/MCD (*Fig. 5A*). The proteome of TNFα-treated organoids demonstrated a canonical, response reminiscent of that observed in lipopolysaccharide (LPS) triggered kidney disease models. The TNFα response involved NFκB2 (immune response, cell development, ECM organization) and TNFα response-specific proteins such as VCAM1, ICAM1, GBP1, ARHGEF2 as well as kinases such as MAP4K4 (implicated in inflammation, programmed cell death), SLK (cell differentiation) and ILK (aging, ECM organization, cell development). Several transcription factors were enriched with TNF exposure, including EGLN1 (also known as PHD2, a hypoxia inducible factor). To further assess the impact of TNFα stimulation on organoids, we also evaluated the secretome (proteins secreted by organoids). We showed that organoids secrete more than 100 proteins, among these CXCL10, a protein active in many autoimmune diseases [33] and papilin, an extracellular matrix glycoprotein, with unknown kidney relevance [34]. Detection of other proteins known to be associated with kidney disease (including complement proteins, proinflammatory extracellular matrix, and cytokines) was also enhanced in TNFα-treated organoid proteome.

In total, our proteomics analysis revealed 320 proteins differentially expressed and/or secreted by TNFα-treated organoids. We showed that summary gene expression of a TNFα gene signature derived from this protein set was significantly higher in a subgroup of individuals with poorer outcomes in FSGS/MCD. This finding adds to our recent study in which we demonstrated that a 272-gene signature derived from a transcriptional analysis of diseased kidney tissue captured the molecular pathobiology of this same subgroup with poorer outcomes. Although on a gene set level, the organoid-based signature demonstrated limited overlap with the tissue-based signature, we attribute this to the focused interrogation of a limited number of cell types in organoids relative to the more heterogeneous cell population of human kidney biopsy tissue, providing a more focused kidney cell-based assessment of protein expression. Moreover, the seemingly disparate gene sets importantly converge on TNFa-centric network, reinforcing the relevance of organoids to FSGS/MCD. Identification of the ten common genes shared between both signatures creates opportunities to: 1) prioritize investigations of molecular pathomechanisms central to FSGS/MCD for disease diagnosis and treatment, 2) identify potential biomarkers for the 272 genes identified in the human kidney signature, as well as 3) align response elements in organoid modeling with human disease for ex vivo testing of potential therapeutics. Additionally, half of these proteins were secreted, raising the potential for identification of additional serum or urine biomarkers of TNFa activity in human kidney disease.

To this point, we further explored two proteins identified in the TNFα-treated organoid secretome, C3 and VCAM1. We found enhanced expression of these genes in tubular cells from individuals with high TNFα signatures (by snRNA-seq), as would be expected of a kidney tissue-derived biomarker. C3 was part of a robust, orchestrated complement secretion response, which included classical cascade components C1q, C1s and C3. Both C1 complex and C3 have been suggested to control aging, apoptosis regulation and cell differentiation [35]. Kidney tubule cells produce C3 mRNA in injury [36] and express proteins C1s and C1r in tubules and glomeruli [37–39]. VCAM-1 is a marker of proximal tubule cells that transition to more regenerative cell types upon injury [40], and negatively associated with glomerular filtration rate in DKD [41] and lupus nephritis [42]. Whether C3 and VCAM1 are causative or reliable markers of disease progression is yet to be determined. Further investigation into what the remaining 310 genes of the organoid TNFα signature could reveal about pathomechanisms of FSGS/MCD is also of interest.

Beyond the functionality of our TNFa organoid model, the combined proteomic and transcriptomic evidence presented here also confirmed that organoids express proteins involved in genetic diseases including ciliopathies autosomal dominant polycystic kidney disease (ADPKD) and autosomal recessive polycystic kidney disease (ARPKD), namely GANAB3 and PKHD1 in addition to PKD1, PKD2 [25,43]. However, the most prominently expressed proteins were related to podocytopathies: more than 300 OMIM referenced disease-related proteins were expressed in organoids, including 65% of all known genes mutated in FSGS/nephrotic syndrome. Organoids also expressed proteins involved in congenital anomalies of the kidney and urinary tract (CAKUT), proteins related to metabolic diseases such as Fanconi syndrome (using the expressed HNF4A nuclear hormone receptor) as well as several metabolic storage diseases (M. Fabry, Galactosemia, GM1-Gangliosidosis, McArdle disease, Niemann-Pick disease)

raising the potential for organoid modeling of these diseases. Furthermore, proteins related to cystinosis [44] immunodeficiency, porphyria and hyperoxaluria were also expressed, supporting development of personalized disease models of kidney phenotypes[7,45]. Yet, we were unable to detect expression of many tubule-specific proteins such as glucose transporter SGLT2 in our organoids, as well as almost all proteins that are known to be expressed in cells in the collecting duct. However, as we demonstrated with TNFRSFA1 expression (*Figs. 4A,B*), some proteins may escape detection using our current proteomics technologies, especially tubular transport genes with limited regions of expression within the kidney tubule. Specialized proteomics protocols or alternative methods such as immunostaining or immunoblotting are needed to examine or model these important metabolic functions [20].

These findings support the use of organoids to model complex human kidney diseases. Firstly, many monogenetic kidney disease markers map to the organoid proteome (*Fig. 7A*). These are chiefly focused on the FSGS/Nephrotic syndrome spectrum and were strongly represented in the data set, covering about 60–65% of OMIM-mentioned FSGS-associated genes, followed by genes responsible for ciliopathies (nephronophthisis, Joubert, Bardet-Biedel Syndrome). Secondly, more complex changes in extracellular matrix are modeled in the organoids, enabling comparisons to multiple diseases in which fibrosis is a prominent feature (*Fig. 7B/C)*. Indeed, our study adds to recent analyses of glomerular basement membrane (GBM) composition of glomeruli of kidney organoids [6,15]. Thirdly, protein-level expression of multiple signaling receptors (*Suppl. Table 13*) facilitates further investigations into pathomechanisms as well as therapeutics. However, it is important to note that kidney organoids dramatically alter their proteome over several days' duration in culture (*Fig. 1*), which could greatly impact disease modeling, emphasizing the need for consistent experimentation. To provide insights in the organoid data acquired here, together with other datasets of glomerular diseases, we made these available through an online application (https://kidneyapp.shinyapps.io/kidneyorganoids/) (*Suppl Fig. 5A*).

In conclusion, organoids can contribute to our understanding of kidney disease in general through integration with human data and pre-clinical models to drive better kidney outcomes for patients (*Fig. 7D*). We demonstrate that hPSC-kidney organoids can be manipulated to capture critical elements of more complex and heterogeneous responses of human kidney disease. Our omic map shows that both inflammation and (related) fibrosis can be rapidly triggered in organoids even in the absence of immune cells. This opens the door to modeling more complex disease where multiple insults may lead to cumulative damage associated with chronic kidney disease. We suggest that other kidney disease researchers can integrate our datasets with their own to improve and refine the generation of kidney disease-relevant organoids as the technology matures further towards full drug discovery and biomarker potential.

# Material And Methods

**Organoid culture, TNFα treatment and sample preparation.** UM77-2 human embryonic stem cells (NIH registration #0278) were cultured in accordance with University of Michigan's Human Pluripotent Stem Cell Research Oversight Committee and NIH regulations, and kidney organoids were generated as

previously described [18]. Organoid cultures (whole wells of cells, isolated spheroids and/or overlying culture medium) were collected at indicated time points: days 21–29 from seeding. For TNFα experiments, almost all samples were collected on D25 following treatment with 5 ng/ml recombinant human TNF-alpha (R&D Systems, cat#10291TA050) reconstituted in DPBS (Gibco, cat#14190144; vehicle control) for 24 or 48 h (medium replenished every 24 h) before collection. Samples collected for scRNA-seq were collected on D24 following 24h TNFa treatment. For proteomics studies, isolated organoids (20 organoids/sample in triplicate) were harvested and washed with ice-cold PBS, and organoid culture medium was collected and snap frozen. For ELISA studies, whole well lysates were prepared by washing the organoids in ice-cold PBS and scraping into Cell Lysis Buffer 2 (R&D Systems, cat#895347) supplemented with Halt Protease and Phosphatase inhibitor Cocktail (Thermo, cat#78440) and medium from corresponding wells was collected and snap frozen. For qRT-PCR/Bulk RNA-seq, whole wells or isolated spheroids were washed, scraped into ice-cold PBS, pelleted and lysed in 500 µL of TRIzol (Invitrogen, cat#15596026) and then total RNA was extracted using Directzol RNA Mini Prep Plus kit (Zymo Research, cat# R2072), as per manufacturer's instructions.

**Organoid immunofluorescence.** Organoid spheroids were fixed in 4% paraformaldehyde (Electron Microscopy Sciences, cat#15710), subjected to a sequential gradient of sucrose, and embedded in 20% sucrose/OCT at ratio 2:1 (Tissue-Plus, ThermoFisher Scientific, cat#4585). 5µm cryosections were rehydrated and blocked with 5% normal donkey serum (Jackson ImmunoResearch Laboratories, cat#017-000-121) in PBS supplemented with 0.1% Triton X-100 (IBI Scientific, cat#IB07100). Slides were immunostained with primary antibodies in 3% BSA (Fraction V, Gibco, cat#15260-037) followed by appropriate Alexa Fluor secondary antibodies (Invitrogen) and mounted using Prolong Gold with DAPI (Invitrogen, cat#P36935). Samples were imaged using a Nikon A1 High Sensitivity Confocal Microscope at the University of Michigan's Microscopy Core and processed with Nikon Elements software. Primary antibodies: N-Cadherin (R&D, cat#AF6426, 1:1000); ACTA2 (R&D, cat#MAB1420-SP, 1:50); PDGFRA (BD Biosciences, cat#556001, 1:200); Synaptopodin (Progen, cat#690094S, 1:80); NPHS1 (R&D, cat#AF4269, 1:500); TNFARSF1A (R&D, cat#MAB225SP, 1:20); VCAM1 (Invitrogen, cat#MA5-11447, 1:50).

**Organoid ELISA.** Protein levels in kidney organoid culture media and lysates were measured using commercially available ELISA kits for IP-10 (R&D Systems, cat#DIP100), MCP-1 (R&D Systems, cat# DCP00), TIMP-1 (R&D Systems, cat# DTM100), C3 (Abcam, cat#ab108823) and VCAM1 (R&D, cat# DVC00). Samples were processed in duplicate following the manufacturer's protocol. Values were normalized to total protein content using Pierce BCA protein assay (Thermo Scientific, cat# 23227). Three independent experiments were performed and plotted using GraphPad Prism software. Statistical significance was calculated using Student's t Test.

**Organoid qRT-PCR.** Total RNA was collected from whole well organoid cultures. One µg of total RNA was reverse-transcribed into cDNA using SuperScript First-Strand Synthesis kit (Invitrogen, cat# 11904018) per manufacturer's protocol. Quantitative real-time PCR (qRT-PCR) was performed using TaqMan Fast Universal PCR Master Mix (2X) (Applied Biosystems, cat# 4352042) in a QuantStudio 7 Flex Real-Time PCR System (ThermoFisher) using TaqMan Pre-Developed Assay Reagents (PDARs) as follows: C3,

Hs00163811_m1; CXCL10, Hs00171042_m1; GAPDH, Hs03929097_g1; VCAM1, Hs01003372_m1. The ΔΔCq method [46]was applied to calculate the relative quantity (RQ) of target gene after normalization to GAPDH. Samples were assayed in duplicate. Graphs of three independent experiments were plotted using GraphPad Prism software. Statistical significance was calculated using Student's t-test.

**Organoid bulk RNA-seq and bioinformatic analysis.**

Organoid bulk RNA-seq and bioinformatic analysis. Total RNA from isolated organoid spheroids was prepared as described above. Library preparation using NEBNext Ultra II kit and sequencing using paired end read length of 150 bases on a NovaSeq4000 were performed by the University of Michigan Advanced Genomics Core. Fastq read quality was determined using FastQC (http://www.bioinformatics.babraham.ac.uk/projects/fastqc/), and reads aligned to the reference (ENSEMBL GRCh38.104) using STAR 2.7.8a [47]. Uniquely mapped reads were inspected for unusual distribution across known annotated features using Picard Tools (https://broadinstitute.github.io/picard/). Gene level read counts were generated using HTSeq (version0.12.4) [48] and normalized with voom [49]. PCA and hierarchical clustering were used to identify and remove samples with abnormal expression profiles due to technical issues, and the mapping statistics obtained from STAR. The data are submitted to GEO (pending accession ID: GSExxxxx).

**Organoid scRNA-seq and bioinformatic analysis.** Whole well organoid cultures were harvested and dissociated as previously described [18]. Single cell suspensions were submitted to the Advanced Genomics Core at the University of Michigan for library preparation and sequencing on a 10x Genomics Chromium System. Organoid scRNA-seq data processing was performed using Seurat 4.0 [50]. Cells expressing > 500 genes were included in the analysis. The processing steps include log transformation, scaling or linear transformation using default settings, highly variable gene identification, dimensionality reduction using principal component reduction (PCA) and Uniform Manifold Approximation and Projection (UMAP), batch correction using harmony function embedded in Seurat and unsupervised clustering at 0.25 resolution. Data deposited here: http://18.188.163.197/

**Proteomics sample preparation, organoids trajectory.** Cell pellets (20 isolated organoid spheroids/sample in triplicate) were lysed using urea buffer containing urea (8M) and ammonium bicarbonate (100 mM) supplemented with 1X PPI (Thermo Scientific Halt Protease and Phosphatase Inhibitor Cocktail). Protein lysates were sonicated for 30 s on 10% power. After centrifugation at 1,400 rpm for 30 min at 4°C, the supernatant was transferred to a new tube. Protein concentrations were measured using a commercial BCA kit (Thermo Scientific, Waltham, MA). The samples were incubated with DTT (10 mM) followed by iodacetamide (40 mM) for 1 h at room temperature for the reduction and alkylation of disulfide bonds. Protein from each sample was digested with trypsin using a 1:100 ratio (1 µg trypsin per 100 µg protein). Digestion was stopped the next day by acidifying to pH 2–3 using formic acid.

**Proteomics analysis, organoids trajectory.** For time-course analysis of organoid cell pellets, peptides were purified using in-house made stage-tips. For nLC-MS/MS analysis of proteomic data, we used a Q

Exactive Plus (Thermo) instrument coupled to a nLC, with a 2.5-h gradient. A binary buffer system with buffer A: 0.1% formic acid (FA) and Buffer B 80% Acetonitrile (ACN) was used. The flow rate was 250 nl/min. The gradient settings were as follows t = 0 min; 4% (Buffer B), 05 min, 6%; 125 min, 23%; 132 min, 54%; 138 min, 85%; 143 min, 85% and 145 min 5%. The flow rate was constant with 250 nL/min. The Q Exactive Plus was operated in positive ion mode. One survey scan (resolution = 70000, m/z 300–1750) was followed by up to 10 MS2 scans (resolution = 17500, m/z 200–2000). Dynamic exclusion was enabled (20 s). AGC target was 3e6 for MS1 scans, and 5e5 for MS2 scans. MS data was processed using MaxQuant as described below. The mass spectrometry proteomics data have been deposited to the ProteomeXchange Consortium via the PRIDE [40] partner repository with the dataset identifiers. Project Name: LC MS/MS of kidney organoids during differentiation from day 21 to 29 Project accession: PXD029716 Project DOI: Not applicable Reviewer account details: Username: reviewer_pxd029716@ebi.ac.uk, Password: y2wNauaO

**Integration of organoid trajectory proteome and transcriptome.** The proteomic data analysis was performed using the Perseus software suite [51] and R [52] for differential expression analysis, GO-term analysis and plotting heatmaps. For trajectory analysis, raw LFQ data were log2 transformed. Missing data was accepted at a threshold of 33% across samples, with subsequent imputation of missing data. Imputation was carried out sample wise with a width of 0.3 SD and a downshift of 1.8 SD as implemented in the Perseus software. Groups were compared using t-tests adjusted for multiple comparisons (permutation-based FDR 0.05), as implemented in the Perseus software. Heatmaps and clustering were carried out in Perseus or in R software via the complexHeatmap package[32] using mean-subtracted data and maximum distance clustering. GO-term annotation of proteins and GO-term enrichment of the heatmap clusters was carried out in Perseus and enrichment assessed by Fisher's exact test. Volcano plots for relevant comparisons were also generated in Perseus. Correlation analysis between protein and bulk RNA transcript was carried out in Perseus. 2D GO-enrichment was also carried out using bulk RNA-seq and bulk proteomics data, with enrichment terms plotted against each other[33]. For integration with scRNA-seq, cell type marker genes from organoid scRNA-seq were used to map protein dynamics indicative of cell type.

**Proteomic analysis of TNFa-treated organoids.** Cell pellets (20 isolated organoid spheroids /sample in triplicate) were lysed using 1:1 4% SDS/0.1M HEPES pH 7.4/5mM EDTA, complemented with protease inhibitor cocktail (Roche) and denaturation at 95°C for 5min. 10 mM TCEP and 50 mM CAA were used for reduction/alkylation of the samples. 50µg aliquots were purified with paramagnetic, mixed 1:1 hydrophobic:hydrophilic SP3 beads [53]. Purified proteins were resuspended in 50 mM HEPES, pH 7.4 and digested over night at 37°C with trypsin (Serva) in a 1:100 (w/w) ratio. Samples were acidified with 2% formic acid and peptides were purified using in-house made stage-tips. Peptides were separated on an Ultimate3000 RSLC nanoHPLC coupled on-line to an Exploris480 orbitrap tandem mass spectrometer (Thermo). The HPLC was operated in a two-column setup with an Acclaim 5mm C18 cartridge pre-column (Thermo) and an ionopticks aurora 25cm column with integrated emitter tip. Separation was performed at 400 nL/min in a heated column oven at 50°C (Sonation) with the following gradient of solvents A

(H2O + 0.1% FA) and B (ACN + 0.1% FA): 120 min from 2–30% B and a high-organic washout at 90% B for 9 min followed by a re-equilibration to the starting conditions (2% B). The mass spectrometer was operated with the FAIMS device at standard resolution with a total carrier glas flow of 3.8 L/min at three CVs: -40, -55 and − 75V. The Orbitrap resolution for the MS1 full scan was set to 120k, whereas the MS2 scans were recorded with 1.5s cycle time for − 40V CV and 0.75s cycle time for − 55/-70V FAIMS CVs at an orbitrap resolution of 15k. Dynamic exclusion mode was set to custom with a 40s exclusion window and a mass tolerance of 10 ppm each.

To assess the organoid secretome, proteins within the overlying cull culture medium of organoid spheroids were denatured using 1:1 4% SDS/0.1M HEPES pH 7.4/5mM EDTA, complemented with protease inhibitor cocktail (Roche) and heating at 95°C for 5 minutes. 10 mM TCEP and 50 mM CAA were used for reduction/alkylation of the samples. 50 µg aliquots were purified with paramagnetic, mixed 1:1 hydrophobic:hydrophilic SP3 beads [35]. Purified proteins were resuspended in 50 mM HEPES, pH 7.4 and digested over night at 37°C with trypsin (Serva) in a 1:100 (w/w) ratio. Samples were acidified with 2% formic acid. All peptides were purified using in-house made stage-tips. The mass spectrometry proteomics data have been deposited to the ProteomeXchange Consortium via the PRIDE [40] partner repository with the dataset identifiers. Project Name 1 (organoid spheroid cell lysate): Proteome analysis of kidney organoid cells during TNFα stimulation Project accession: PXD029718 Project DOI: 10.6019/PXD029718 Reviewer account details: Username: reviewer_pxd029718@ebi.ac.uk Password: tdei7cSf. Project Name 2 (secretome): Proteomic analysis of kidney organoid supernatant during TNFα stimulation Project accession: PXD029696 Project DOI: 10.6019/PXD029696 Reviewer account details: Username: reviewer_pxd029696@ebi.ac.uk Password: jKHFtF9T

**Organoid proteome data processing.** For organoid trajectory samples, raw files were searched, quantified and normalized using the MaxQuant [29] version 1.5.3.8 (FDR = 1%). Label-free quantification [29], intensity based absolute quantification (iBAQ) with log fit, and the match-between-runs feature were enabled. We used the UniProt human reference proteome as database (downloaded in January 2017) and default settings for orbitraps. Enzyme specificity was set to Trypsin/P, cysteine carbamidomethylation was set as a fixed modification (+ 57.021464) and methionine oxidation (+ 15.994914) as well as protein N-terminal acetylation (+ 42.010565) were set as variable modifications. Data analysis was performed using Perseus software suite (V1.5.1.6). For organoid TNFα experimental samples, raw FAIMS data were converted into MzXML files with the FAIMS_MzXML_Generator tool (v1.0.7639, [36]) and queried with MaxQuant v 1.6.7.0 (FDR = 1%, match between runs = on) using the UniProt reference proteome database for human (May 2020, canonical only, 20600 entries) and default settings for orbitrap instruments. Enzyme specificity was set to Trypsin/P, cysteine carbamidomethylation was set as a fixed modification (+ 57.021464) and methionine oxidation (+ 15.994914) as well as protein N-terminal acetylation (+ 42.010565) were set as variable modifications. The match-between-runs feature was activated with default settings.

**Organoid proteome data analysis.** The data analysis was performed using the Perseus software suite and R for GO-term analysis. For organoid trajectory sample analysis and for GO-term annotation, raw LFQ

data were log2 transformed, triplicates were averaged, and proteins detected on all four days of differentiation were used. For volcano plotting and t-tests individual samples were used with missing data accepted at a threshold of 33% across samples, with subsequent imputation of missing data. Imputation was carried out sample wise with a width of 0.3 SD and a downshift of 1.8 SD as implemented in the Perseus software. GO terms were annotated and between group testing was carried out using Student's t-test and Volcano plots for relevant comparisons. For organoid TNFα experimental samples, data were log2 transformed and GO-terms annotated, data were filtered to only include proteins for which we had complete data in 3 of 3 replicates within at least one group with subsequent imputation of missing data. Imputation was carried out sample wise with a width of 0.3 SD and a downshift of 1.8 SD. The FDR for Volcano plots was held at 0.05 for the trajectory analysis, at 0.1 for TNFα treated organoids. For GO term enrichment we used Fisher Exact testing implemented in Perseus (FDR 0.05) or the Enrichr R package (adjusted p-value < 0.05 as significant). Top GO terms per annotation term category were then used for plotting. Heatmaps and clustering were carried out in Perseus using mean-subtracted data and maximum distance clustering or using the R package complexHeatmap [32]. Venn diagrams were generated using gene symbols of the relevant data sets and produced using the Rvennr package. GO-term annotation of intersecting and unique Venn sections was performed using EnrichR. 2D scattering of RNA count vs protein IBAQ and keyword analysis was carried out in Perseus software with visualization of 2xSD in R. UMAP and marker lists of scRNA-seq were produced using the Seurat R package. Matrisome networks were generated from proteins in our dataset annotated with matrisome as a uniprot keyword. A list of matrisome associated identifiers was uploaded to string-db.org (V.11.0) with standard settings and 'highest confidence' selected for the minimum required interaction score. The STRING database[54] was used to generate the network which was then imported into Cytoscape (V 3.8.2)[55] and log2 fold changes mapped to the network indicating magnitude of the fold change through size and directionality through color. To assess to which degree organoids express disease relevant proteins, we mapped proteins between OMIM disease genes and organoids.

**Human podocyte culture.** Human podocytes[56] were cultured in dishes as previously described and regularly tested for mycoplasma using a commercial kit (LookOut, Sigma). 50,000 cells were seeded in 6-well dishes (Thermo Scientific) and cultured at 32°C with 5% $CO_2$ in RPMI 1640 (Gibco, Thermo Scientific) containing 10% FBS (Gibco, Thermo Scientific), 1% Penicillin-Streptomycin (Gibco, Thermo Scientific), 1% insulin-transferrin-sodium selenite (Thermo Scientific), 1% MEM (Gibco, Thermo Scientific), 1 mM Sodiumpyruvate (Gibco, Thermo Scientific) and 20 mM HEPES (Gibco, Thermo Scientific). 24 h after seeding, cells were washed once with PBS and medium was replaced with FBS-free medium containing 5 ng/mL TNFα (R&D Systems, same vendor as for organoid treatment) or vehicle control. After 24 or 48 h, culture medium was removed and snap frozen. Cells were washed twice with PBS and scraped into ice-cold urea buffer (8M urea, 100 mM ammonium bicarbonate, 1X PPI), snap frozen and stored until analysis.

**Analysis of the human cultured podocyte proteome.** Cells and supernatants were analyzed using MaxQuant and Perseus. Raw files were searched, quantified, and normalized using MaxQuant version

1.6.17.0 with default settings for orbitraps. The match between runs (MBR), LFQ, IBAQ and classical normalization features were enabled. We used the UniProt human reference proteome as database (UP000005640_9606, downloaded in April 2021 with 20612 entries with enzyme specificity set to Trypsin/P, cysteine carbamidomethylation as a fixed modification (+ 57.021464) and methionine oxidation (+ 15.994914) as well as protein N-terminal acetylation (+ 42.010565) were as variable modifications. Data analysis was performed using Perseus software suite (V1.6.2.3). TNFα-treated podocyte data were log2 transformed and filtered to only include proteins that were measured in at least 4 out of 6 replicates in at least one group. Missing data was imputed sample wise from a normal distribution with a width of 0.3 SD and a downshift of 1.8 SD. Volcano plots were created according to a two-sided t-test with an FDR of 0.2 for supernatants and an FDR of 0.1 for cells. The mass spectrometry proteomics data have been deposited to the ProteomeXchange Consortium via the PRIDE [40] partner repository with the dataset identifiers. Project Name 1 : Proteomic analysis of cultured human podocytes stimulated with TNFα - cell pellet, Project accession: PXD032107 Project DOI: Not applicable, Reviewer account details: Username: reviewer_pxd032107@ebi.ac.uk Password: TCWTgTMa. Project Name 2: Proteomic analysis of cultured human podocytes stimulated with TNFα – supernatant, Project accession: PXD032130, Project DOI: Not applicable,Reviewer account details: Username: reviewer_pxd032130@ebi.ac.uk, Password: j2wELsGJ

**Human glomeruli and tubule proteomics data.** Datasets were retrieved for human microdissected proximal tubules and single human glomeruli from adult human kidneys [19] to compare with our organoid data.

**Deep proteomic analysis of human glomeruli.** For deep mass spectrometry analysis sieved human glomeruli were used as previously described [34]. Proteins from glomeruli were extracted, solubilized and trypsinized as described above. The tryptic digests were fractionated using in-house made stage-tips, applying high pH reverse phase fractionation with fresh 100 mM ammonium formate, pH 10 and stepwise increase of ACN from 0–50% (n = 8 fractions). The eight fractions were analyzed on the same Q Exactive Plus instrument as indicated above with analogous settings.

**NEPTUNE bulk RNA-seq and snRNA-seq.** Data from an existing study of individuals with proteinuric kidney disease were utilized for analysis [24]. In brief, the NEPTUNE (NCT01209000) study objectives, design and procedures were described in previous publications [57,58]. Consent was obtained from individuals or parents/guardians at enrollment, and the study was approved (HUM00158219) by University of Michigan, Medical School Institutional Review Board. Renal biopsies were microdissected into glomeruli and tubulointerstitial compartments. Bulk tubulointerstitium kidney biopsy transcriptional data from 220 NEPTUNE participants with FSGS/MCD are available through via GEO accession number GSE182380. Single nuclear transcriptional data for ten NEPTUNE participants within this cohort, five with high intrarenal TNF activity and five with low TNF activity, are available via GEO accession number GSE213030.

**Organoid derived proteomic TNF signature applied to NEPTUNE kidney tissue transcriptome data.** The proteomic signatures of TNFα treated organoids were derived from the total of 320 differentially expressed proteins (DEPs) under TNFα treatment at 24 and 48 h (*supplemental table 10*) by combining cellular proteins (n = 300 DEPs) plus those proteins secreted into the culture medium (n = 22 DEPs) (*supplemental tables 3 and 4*), 2 DEPs were represented in both sets. Peptide to ENSEMBL gene id conversions were performed using Biomart. In cases where peptides mapped to more than one protein, each gene encoding the given protein was used for the gene set. Each of the three gene sets (cellular, secreted, combined) was used to compute an eigengene (first principal component) from each patient-derived tubulointerstitial transcriptome profile in patients with MCD or FSGS from NEPTUNE (GSE140989).

**TNF network and pathway analysis.** For each of the two gene signatures, i) from the previously characterized TNF gene set in human kidney tissue (n = 272 genes) [24], ii) from the organoid TNFα proteome (n = 320 genes) and the combination of these two gene signatures (n = 582 genes), biologic literature-based networks were generated using Genomatix Pathway System (GePS) software (http://genomatix.de). In these networks, the 100 best connected genes co-cited in PubMed abstracts in the same sentence linked to a function word (most relevant genes/interactions) were represented. The TNF-centric network was generated from the 582 combined genes asking the software to include in the network the 10 common genes listed in *Fig. 5B* in the 100 best connected genes. The top 20 pathway-based and signal transduction networks were generated from the individual and combined gene signatures using GePS (*Suppl. Tables 11 and 12*).

**Transcriptomic analysis of the European Renal cDNA Bank (ERCB) tissue.** Previously generated microarray data from microdissected human glomeruli and tubulointerstitium sourced from individuals with kidney disease (n = 184) and healthy donors (n = 50) were used (GEO accession # GSE104948 and GSE104954) [59].Microarray assays captured a subset of 267 genes of the 320-gene product kidney organoid signature in the ERCB cohort. Gene expression was Z-transformed, and Z-scores were calculated as previously described [24].

**Kidney Disease Explorer Shiny application.** Seventeen different data sets from the following prior publications were combined with data from this study for this application. Rinschen et al. [37] defined the cellular effects of puromycin aminonucleoside (PAN) under different circumstances (in vitro differentiated and non-differentiated, in vivo after two and four days). Höhne et al. [19] created proteomic datasets for various kidney diseases (FSGS, congenital nephrotic syndrome) based on individual kidney segments. Bartram et al. analyzed FSGS (podocyte cell line and primary renal epithelial cells from urine) due to G195D mutation in the ACTN4 gene[38]. Koehler et al. analzyed the effects of doxorubicin and LPS on podocytes[39]. The app is available at https://kidneyapp.shinyapps.io/kidneyorganoids/.

**Western blot for complement factor C3.** Proteins in culture media were separated on 4–15% gradient SDS-PAGE gels (Bio-Rad, Criterion TGX gels #567–1083) and transferred to nitrocellulose membranes (Bio-Rad #170–4159) which was blocked and developed with polyclonal rabbit anti-human-C3c (DAKO

#0368) in Tris-buffered saline, 1 mM EDTA, pH 7.4, with 1 mg human serum albumin (CSL Behring #109697) and 100 µg human IgG (CSL Behring #007815) per milliliter. The membrane was then washed, incubated with horseradish peroxidase-conjugated goat anti-rabbit IgG antibody (DAKO #P0448) and developed with SuperSignal West Dura extended-duration substrate (Pierce). Emission was recorded by a charge-coupled device camera.

# Declarations

### Author Contributions

All co-authors have contributed to the manuscript.

JLH, MMR conceptualized and supervised this study

ML, JLH, MMR wrote the original draft.

ML, SFE, JE, MF, CCB, VV did the formal analysis.

SFE, JE, MF, CCB, RM, VV, WJ developed the methodology.

ML, SFE, AH, CCB, LLB, RM, FE, FA, DF, PJM, BG performed bioinformatic processing and analyses in the study.

JE, MF, VV performed kidney organoid experiments (including generating & analyzing qPCR, ELISA, IF data).

FD performed proteomics.

ML, SFE, JE, MF, AH, LLB, VV, PB contributed to data curation.

BD, LR performed cell culture (separate from organoids) or worked on human glomeruli isolation.

ML, SFE, AH, CCB, RM, FA, DF, PJM, FD helped with visualization.

ML, SFE, JLH, MMR were involved in project administration.

EH, FG, MTL, TBH, HS, ST, LHM, MK provided resources.

FG, TBH, MK, FD, JLH, MMR were involved in funding acquisition.

All authors reviewed and provided valuable feedback on the manuscript.

**Acknowledgements.** The authors extend their gratitude to investigators and participants involved in the ERCB and the NEPTUNE consortia and data made available through funding and/or programmatic

support to NEPTUNE provided by the NephCure Kidney International and the Halpin Foundation. The authors acknowledge excellent technical support by Stefan Gatzemeier, Mette Løbner, Yuee Wang and Emily Tanner. The Nephrotic Syndrome Study Network (NEPTUNE) is part of the Rare Diseases Clinical Research Network (RDCRN), which is funded by the National Institutes of Health (NIH) and led by the National Center for Advancing Translational Sciences (NCATS) through its Division of Rare Diseases Research Innovation (DRDRI). NEPTUNE is funded under grant number U54DK083912 as a collaboration between NCATS and the National Institute of Diabetes and Digestive and Kidney Diseases (NIDDK). Additional funding and/or programmatic support is provided by the University of Michigan, NephCure Kidney International and the Halpin Foundation. RDCRN consortia are supported by the RDCRN Data Management and Coordinating Center (DMCC), funded by NCATS and the National Institute of Neurological Disorders and Stroke (NINDS) under U2CTR002818.

### Disclosures

**Funding** MMR was supported by the DFG (RI 2811/1-1 and RI 2811/2-1, and SFB1192-project B10), by the Young Investigator Award from the Novo Nordisk Foundation, grant number NNF19OC0056043, the Carlsberg Young Investigator fellowship as well as Aarhus universitet forskningsfond. This project has received funding from the European Union's Horizon 2020 research and innovation programme under the Marie Skłodowska-Curie grant agreement No 754513 and The Aarhus University Research Foundation (to M.M.R). JLH and MK are supported by NIH NCATS UG3-TR-003288-01 and JDRF. BD received intramural funding from the UKE (Clinician Scientist Program). FG received DFG funding (DFG GR3933/1-1, SFB 1192 B 09). EH received funding through the Heisenberg-Program of the DFG (DFG 414280945). SFE, RM, CCB, FE, BG, FA, PJM, DF, WJ are supported by the University of Michigan O'Brien Center Applied Systems Biology Core (P30 DK081943). The NEPTUNE consortium, U54-DK-083912, is part of the National Institutes of Health Rare Disease Clinical Research Network, supported through a collaboration between the Office of Rare Diseases Research, National Center for Advancing Translational Sciences, and the National Institute of Diabetes and Digestive and Kidney Diseases.

## References

1. Czerniecki SM, Cruz NM, Harder JL, Menon R, Annis J, Otto EA, Gulieva RE, Islas LV, Kim YK, Tran LM, et al. High-Throughput Screening Enhances Kidney Organoid Differentiation from Human Pluripotent Stem Cells and Enables Automated Multidimensional Phenotyping. Cell Stem Cell. 2018;22:929–940.e924. doi: https://doi.org/10.1016/j.stem.2018.04.022
2. Tanigawa S, Islam M, Sharmin S, Naganuma H, Yoshimura Y, Haque F, Era T, Nakazato H, Nakanishi K, Sakuma T, et al. Organoids from Nephrotic Disease-Derived iPSCs Identify Impaired NEPHRIN Localization and Slit Diaphragm Formation in Kidney Podocytes. Stem Cell Reports. 2018;11:727–740. doi: https://doi.org/10.1016/j.stemcr.2018.08.003
3. Nishinakamura R. Human kidney organoids: progress and remaining challenges. Nature Reviews Nephrology. 2019;15:613–624. doi: 10.1038/s41581-019-0176-x

4. Calandrini C, Schutgens F, Oka R, Margaritis T, Candelli T, Mathijsen L, Ammerlaan C, van Ineveld RL, Derakhshan S, de Haan S, et al. An organoid biobank for childhood kidney cancers that captures disease and tissue heterogeneity. Nature Communications. 2020;11:1310. doi: 10.1038/s41467-020-15155-6
5. Forbes TA, Howden SE, Lawlor K, Phipson B, Maksimovic J, Hale L, Wilson S, Quinlan C, Ho G, Holman K, et al. Patient-iPSC-Derived Kidney Organoids Show Functional Validation of a Ciliopathic Renal Phenotype and Reveal Underlying Pathogenetic Mechanisms. The American Journal of Human Genetics. 2018;102:816–831. doi: https://doi.org/10.1016/j.ajhg.2018.03.014
6. Morais MRPT, Tian P, Lawless C, Murtuza-Baker S, Hopkinson L, Woods S, Mironov A, Long DA, Gale DP, Zorn TMT, et al. Kidney organoids recapitulate human basement membrane assembly in health and disease. eLife. 2022;11:e73486. doi: 10.7554/eLife.73486
7. Jansen J, van den Berge BT, van den Broek M, Maas RJ, Willemsen B, Kuppe C, Reimer KC, Giovanni GD, Mooren F, Nlandu Q, et al. Human pluripotent stem cell-derived kidney organoids for personalized congenital and idiopathic nephrotic syndrome modeling. *bioRxiv*. 2021:2021.2010.2027.466054. doi: 10.1101/2021.10.27.466054
8. Yang L, Han Y, Nilsson-Payant BE, Gupta V, Wang P, Duan X, Tang X, Zhu J, Zhao Z, Jaffré F, et al. A Human Pluripotent Stem Cell-based Platform to Study SARS-CoV-2 Tropism and Model Virus Infection in Human Cells and Organoids. Cell Stem Cell. 2020;27:125–136.e127. doi: 10.1016/j.stem.2020.06.015
9. Gulieva RE, Higgins AZ. Human induced pluripotent stem cell derived kidney organoids as a model system for studying cryopreservation. Cryobiology. 2021. doi: 10.1016/j.cryobiol.2021.08.006
10. Bock C, Boutros M, Camp JG, Clarke L, Clevers H, Knoblich JA, Liberali P, Regev A, Rios AC, Stegle O, et al. The Organoid Cell Atlas. Nature Biotechnology. 2021;39:13–17. doi: 10.1038/s41587-020-00762-x
11. Sander V, Przepiorski A, Crunk AE, Hukriede NA, Holm TM, Davidson AJ. Protocol for Large-Scale Production of Kidney Organoids from Human Pluripotent Stem Cells. STAR Protoc. 2020;1:100150. doi: 10.1016/j.xpro.2020.100150
12. Przepiorski A, Sander V, Tran T, Hollywood JA, Sorrenson B, Shih JH, Wolvetang EJ, McMahon AP, Holm TM, Davidson AJ. A Simple Bioreactor-Based Method to Generate Kidney Organoids from Pluripotent Stem Cells. Stem Cell Reports. 2018;11:470–484. doi: 10.1016/j.stemcr.2018.06.018
13. Little MH, Howden SE, Lawlor KT, Vanslambrouck JM. Determining lineage relationships in kidney development and disease. Nat Rev Nephrol. 2021. doi: 10.1038/s41581-021-00485-5
14. Shankar AS, van den Berg SAA, Tejeda Mora H, Du Z, Lin H, Korevaar SS, van der Wal R, van den Bosch TPP, Clahsen-van Groningen MC, Gribnau J, et al. Vitamin D metabolism in human kidney organoids. Nephrology Dialysis Transplantation. 2021. doi: 10.1093/ndt/gfab264
15. Hale LJ, Howden SE, Phipson B, Lonsdale A, Er PX, Ghobrial I, Hosawi S, Wilson S, Lawlor KT, Khan S, et al. 3D organoid-derived human glomeruli for personalised podocyte disease modelling and drug screening. Nat Commun. 2018;9:5167. doi: 10.1038/s41467-018-07594-z

16. Morizane R, Bonventre JV. Kidney Organoids: A Translational Journey. Trends in Molecular Medicine. 2017;23:246–263. doi: https://doi.org/10.1016/j.molmed.2017.01.001
17. Freedman BS. Physiology assays in human kidney organoids. Am J Physiol Renal Physiol. 2022;322:F625-f638. doi: 10.1152/ajprenal.00400.2021
18. Harder JL, Menon R, Otto EA, Zhou J, Eddy S, Wys NL, O'Connor C, Luo J, Nair V, Cebrian C, et al. Organoid single cell profiling identifies a transcriptional signature of glomerular disease. JCI Insight. 2019;4. doi: 10.1172/jci.insight.122697
19. Combes AN, Zappia L, Er PX, Oshlack A, Little MH. Single-cell analysis reveals congruence between kidney organoids and human fetal kidney. Genome Medicine. 2019;11:3. doi: 10.1186/s13073-019-0615-0
20. Uchimura K, Wu H, Yoshimura Y, Humphreys BD. Human Pluripotent Stem Cell-Derived Kidney Organoids with Improved Collecting Duct Maturation and Injury Modeling. Cell Reports. 2020;33:108514. doi: https://doi.org/10.1016/j.celrep.2020.108514
21. Subramanian A, Sidhom E-H, Emani M, Vernon K, Sahakian N, Zhou Y, Kost-Alimova M, Slyper M, Waldman J, Dionne D, et al. Single cell census of human kidney organoids shows reproducibility and diminished off-target cells after transplantation. Nature Communications. 2019;10:5462. doi: 10.1038/s41467-019-13382-0
22. Wilson SB, Howden SE, Vanslambrouck JM, Dorison A, Alquicira-Hernandez J, Powell JE, Little MH. DevKidCC allows for robust classification and direct comparisons of kidney organoid datasets. Genome Med. 2022;14:19. doi: 10.1186/s13073-022-01023-z
23. Liu Y, Beyer A, Aebersold R. On the Dependency of Cellular Protein Levels on mRNA Abundance. Cell. 2016;165:535–550. doi: 10.1016/j.cell.2016.03.014
24. Mariani LH, Eddy S, AlAkwaa FM, McCown PJ, Harder JL, Martini S, Ademola AD, Boima V, Reich HN, Eichinger F, et al. Multidimensional Data Integration Identifies Tumor Necrosis Factor Activation in Nephrotic Syndrome: A Model for Precision Nephrology. *medRxiv*. 2021:2021.2009.2009.21262925. doi: 10.1101/2021.09.09.21262925
25. Freedman BS, Brooks CR, Lam AQ, Fu H, Morizane R, Agrawal V, Saad AF, Li MK, Hughes MR, Werff RV, et al. Modelling kidney disease with CRISPR-mutant kidney organoids derived from human pluripotent epiblast spheroids. Nature Communications. 2015;6:8715. doi: 10.1038/ncomms9715
26. Hutzfeldt AD, Tan Y, Bonin LL, Beck BB, Baumbach J, Lassé M, Demir F, Rinschen MM. Consensus draft of the native mouse podocyte-ome. Am J Physiol Renal Physiol. 2022. doi: 10.1152/ajprenal.00058.2022
27. Hohne M, Frese CK, Grahammer F, Dafinger C, Ciarimboli G, Butt L, Binz J, Hackl MJ, Rahmatollahi M, Kann M, et al. Single-nephron proteomes connect morphology and function in proteinuric kidney disease. Kidney Int. 2018;93:1308–1319. doi: 10.1016/j.kint.2017.12.012
28. Salomon BL. Insights into the biology and therapeutic implications of TNF and regulatory T cells. Nat Rev Rheumatol. 2021;17:487–504. doi: 10.1038/s41584-021-00639-6

29. Tyanova S, Temu T, Cox J. The MaxQuant computational platform for mass spectrometry-based shotgun proteomics. Nat Protoc. 2016;11:2301–2319. doi: 10.1038/nprot.2016.136
30. Ding J, Adiconis X, Simmons SK, Kowalczyk MS, Hession CC, Marjanovic ND, Hughes TK, Wadsworth MH, Burks T, Nguyen LT, et al. Systematic comparison of single-cell and single-nucleus RNA-sequencing methods. Nat Biotechnol. 2020;38:737–746. doi: 10.1038/s41587-020-0465-8
31. Bakken TE, Hodge RD, Miller JA, Yao Z, Nguyen TN, Aevermann B, Barkan E, Bertagnolli D, Casper T, Dee N, et al. Single-nucleus and single-cell transcriptomes compared in matched cortical cell types. PloS one. 2018;13:e0209648. doi: 10.1371/journal.pone.0209648
32. Little MH, Humphreys BD. Regrow or Repair: An Update on Potential Regenerative Therapies for the Kidney. J Am Soc Nephrol. 2022;33:15–32. doi: 10.1681/asn.2021081073
33. Karin N, Razon H. Chemokines beyond chemo-attraction: CXCL10 and its significant role in cancer and autoimmunity. Cytokine. 2018;109:24–28. doi: 10.1016/j.cyto.2018.02.012
34. Kramerova IA, Kawaguchi N, Fessler LI, Nelson RE, Chen Y, Kramerov AA, Kusche-Gullberg M, Kramer JM, Ackley BD, Sieron AL, et al. Papilin in development; a pericellular protein with a homology to the ADAMTS metalloproteinases. Development. 2000;127:5475–5485.
35. Lu J, Kishore U. C1 Complex: An Adaptable Proteolytic Module for Complement and Non-Complement Functions. Front Immunol. 2017;8:592. doi: 10.3389/fimmu.2017.00592
36. Spath MR, Bartram MP, Palacio-Escat N, Hoyer KJR, Debes C, Demir F, Schroeter CB, Mandel AM, Grundmann F, Ciarimboli G, et al. The proteome microenvironment determines the protective effect of preconditioning in cisplatin-induced acute kidney injury. Kidney Int. 2019;95:333–349. doi: 10.1016/j.kint.2018.08.037
37. Zhou W, Marsh JE, Sacks SH. Intrarenal synthesis of complement. Kidney Int. 2001;59:1227–1235. doi: 10.1046/j.1523-1755.2001.0590041227.x
38. Zhou X, Fukuda N, Matsuda H, Endo M, Wang X, Saito K, Ueno T, Matsumoto T, Matsumoto K, Soma M, et al. Complement 3 activates the renal renin-angiotensin system by induction of epithelial-to-mesenchymal transition of the nephrotubulus in mice. Am J Physiol Renal Physiol. 2013;305:F957-967. doi: 10.1152/ajprenal.00344.2013
39. Uhlén M, Fagerberg L, Hallström BM, Lindskog C, Oksvold P, Mardinoglu A, Sivertsson Å, Kampf C, Sjöstedt E, Asplund A, et al. Proteomics. Tissue-based map of the human proteome. Science. 2015;347:1260419. doi: 10.1126/science.1260419
40. Muto Y, Wilson PC, Ledru N, Wu H, Dimke H, Waikar SS, Humphreys BD. Single cell transcriptional and chromatin accessibility profiling redefine cellular heterogeneity in the adult human kidney. Nat Commun. 2021;12:2190. doi: 10.1038/s41467-021-22368-w
41. Jia Y, Xu H, Yu Q, Tan L, Xiong Z. Identification and verification of vascular cell adhesion protein 1 as an immune-related hub gene associated with the tubulointerstitial injury in diabetic kidney disease. Bioengineered. 2021;12:6655–6673. doi: 10.1080/21655979.2021.1976540
42. Gasparin AA, de Andrade NPB, Hax V, Palominos PE, Siebert M, Marx R, Schaefer PG, Veronese FV, Monticielo OA. Urinary soluble VCAM-1 is a useful biomarker of disease activity and treatment

response in lupus nephritis. BMC Rheumatol. 2020;4:67. doi: 10.1186/s41927-020-00162-3

43. Cruz NM, Song X, Czerniecki SM, Gulieva RE, Churchill AJ, Kim YK, Winston K, Tran LM, Diaz MA, Fu H, et al. Organoid cystogenesis reveals a critical role of microenvironment in human polycystic kidney disease. Nat Mater. 2017;16:1112–1119. doi: 10.1038/nmat4994
44. Hollywood JA, Przepiorski A, D'Souza RF, Sreebhavan S, Wolvetang EJ, Harrison PT, Davidson AJ, Holm TM. Use of Human Induced Pluripotent Stem Cells and Kidney Organoids To Develop a Cysteamine/mTOR Inhibition Combination Therapy for Cystinosis. J Am Soc Nephrol. 2020;31:962–982. doi: 10.1681/asn.2019070712
45. Morais MRPT, Tian P, Lawless C, Murtuza-Baker S, Hopkinson L, Woods S, Mironov A, Long DA, Gale D, Zorn TMT, et al. Kidney organoids: A system to study human basement membrane assembly in health and disease. *bioRxiv*. 2021:2021.2006.2027.450067. doi: 10.1101/2021.06.27.450067
46. Livak KJ, Schmittgen TD. Analysis of relative gene expression data using real-time quantitative PCR and the 2(-Delta Delta C(T)) Method. Methods. 2001;25:402–408. doi: 10.1006/meth.2001.1262
47. Dobin A, Davis CA, Schlesinger F, Drenkow J, Zaleski C, Jha S, Batut P, Chaisson M, Gingeras TR. STAR: ultrafast universal RNA-seq aligner. Bioinformatics. 2013;29:15–21. doi: 10.1093/bioinformatics/bts635
48. Anders S, Pyl PT, Huber W. HTSeq–a Python framework to work with high-throughput sequencing data. Bioinformatics. 2015;31:166–169. doi: 10.1093/bioinformatics/btu638
49. Law CW, Chen Y, Shi W, Smyth GK. voom: Precision weights unlock linear model analysis tools for RNA-seq read counts. Genome Biol. 2014;15:R29. doi: 10.1186/gb-2014-15-2-r29
50. Hao Y, Hao S, Andersen-Nissen E, Mauck WM, 3rd, Zheng S, Butler A, Lee MJ, Wilk AJ, Darby C, Zager M, et al. Integrated analysis of multimodal single-cell data. Cell. 2021;184:3573–3587.e3529. doi: 10.1016/j.cell.2021.04.048
51. Tyanova S, Temu T, Sinitcyn P, Carlson A, Hein MY, Geiger T, Mann M, Cox J. The Perseus computational platform for comprehensive analysis of (prote)omics data. Nat Methods. 2016;13:731–740. doi: 10.1038/nmeth.3901
52. R Core Team. R: A Language and Environment for Statistical Computing. 2018.
53. Weng SSH, Demir F, Ergin EK, Dirnberger S, Uzozie A, Tuscher D, Nierves L, Tsui J, Huesgen PF, Lange PF. Sensitive Determination of Proteolytic Proteoforms in Limited Microscale Proteome Samples. Molecular & cellular proteomics: MCP. 2019;18:2335–2347. doi: 10.1074/mcp.TIR119.001560
54. Szklarczyk D, Gable AL, Nastou KC, Lyon D, Kirsch R, Pyysalo S, Doncheva NT, Legeay M, Fang T, Bork P, et al. The STRING database in 2021: customizable protein-protein networks, and functional characterization of user-uploaded gene/measurement sets. Nucleic Acids Res. 2021;49:D605-d612. doi: 10.1093/nar/gkaa1074
55. Shannon P, Markiel A, Ozier O, Baliga NS, Wang JT, Ramage D, Amin N, Schwikowski B, Ideker T. Cytoscape: a software environment for integrated models of biomolecular interaction networks. Genome Res. 2003;13:2498–2504. doi: 10.1101/gr.1239303

56. Saleem MA, O'Hare MJ, Reiser J, Coward RJ, Inward CD, Farren T, Xing CY, Ni L, Mathieson PW, Mundel P. A conditionally immortalized human podocyte cell line demonstrating nephrin and podocin expression. J Am Soc Nephrol. 2002;13:630–638. doi: 10.1681/asn.V133630
57. Barisoni L, Nast CC, Jennette JC, Hodgin JB, Herzenberg AM, Lemley KV, Conway CM, Kopp JB, Kretzler M, Lienczewski C, et al. Digital pathology evaluation in the multicenter Nephrotic Syndrome Study Network (NEPTUNE). Clin J Am Soc Nephrol. 2013;8:1449–1459. doi: 10.2215/cjn.08370812
58. Gadegbeku CA, Gipson DS, Holzman LB, Ojo AO, Song PX, Barisoni L, Sampson MG, Kopp JB, Lemley KV, Nelson PJ, et al. Design of the Nephrotic Syndrome Study Network (NEPTUNE) to evaluate primary glomerular nephropathy by a multidisciplinary approach. Kidney Int. 2013;83:749–756. doi: 10.1038/ki.2012.428
59. Schmid H, Cohen CD, Henger A, Schlöndorff D, Kretzler M. Gene expression analysis in renal biopsies. Nephrol Dial Transplant. 2004;19:1347–1351. doi: 10.1093/ndt/gfh181
60. Hsieh LT, Nastase MV, Zeng-Brouwers J, Iozzo RV, Schaefer L. Soluble biglycan as a biomarker of inflammatory renal diseases. Int J Biochem Cell Biol. 2014;54:223–235. doi: 10.1016/j.biocel.2014.07.020
61. Stokes MB, Holler S, Cui Y, Hudkins KL, Eitner F, Fogo A, Alpers CE. Expression of decorin, biglycan, and collagen type I in human renal fibrosing disease. Kidney Int. 2000;57:487–498. doi: 10.1046/j.1523-1755.2000.00868.x
62. Stokes MB, Hudkins KL, Zaharia V, Taneda S, Alpers CE. Up-regulation of extracellular matrix proteoglycans and collagen type I in human crescentic glomerulonephritis. Kidney Int. 2001;59:532–542. doi: 10.1046/j.1523-1755.2001.059002532.x
63. Sun XX, Li SS, Zhang M, Xie QM, Xu JH, Liu SX, Gu YY, Pan FM, Tao JH, Xu SQ, et al. Association of HSP90B1 genetic polymorphisms with efficacy of glucocorticoids and improvement of HRQoL in systemic lupus erythematosus patients from Anhui Province. Am J Clin Exp Immunol. 2018;7:27–39.
64. Pockley AG. Heat shock proteins as regulators of the immune response. Lancet. 2003;362:469–476. doi: 10.1016/s0140-6736(03)14075-5
65. Vaidya VS, Niewczas MA, Ficociello LH, Johnson AC, Collings FB, Warram JH, Krolewski AS, Bonventre JV. Regression of microalbuminuria in type 1 diabetes is associated with lower levels of urinary tubular injury biomarkers, kidney injury molecule-1, and N-acetyl-β-D-glucosaminidase. Kidney Int. 2011;79:464–470. doi: 10.1038/ki.2010.404
66. Gao J, Wu L, Wang S, Chen X. Role of Chemokine (C-X-C Motif) Ligand 10 (CXCL10) in Renal Diseases. Mediators Inflamm. 2020;2020:6194864. doi: 10.1155/2020/6194864
67. Arrizabalaga P, Solé M, Abellana R, de las Cuevas X, Soler J, Pascual J, Ascaso C. Tubular and interstitial expression of ICAM-1 as a marker of renal injury in IgA nephropathy. Am J Nephrol. 2003;23:121–128. doi: 10.1159/000068920
68. Singh S, Wu T, Xie C, Vanarsa K, Han J, Mahajan T, Oei HB, Ahn C, Zhou XJ, Putterman C, et al. Urine VCAM-1 as a marker of renal pathology activity index in lupus nephritis. Arthritis Res Ther. 2012;14:R164. doi: 10.1186/ar3912

69. Tu Z, Kelley VR, Collins T, Lee FS. I kappa B kinase is critical for TNF-alpha-induced VCAM1 gene expression in renal tubular epithelial cells. J Immunol. 2001;166:6839–6846. doi: 10.4049/jimmunol.166.11.6839
70. Sartain SE, Turner NA, Moake JL. TNF Regulates Essential Alternative Complement Pathway Components and Impairs Activation of Protein C in Human Glomerular Endothelial Cells. J Immunol. 2016;196:832–845. doi: 10.4049/jimmunol.1500960
71. Low SH, Vasanth S, Larson CH, Mukherjee S, Sharma N, Kinter MT, Kane ME, Obara T, Weimbs T. Polycystin-1, STAT6, and P100 function in a pathway that transduces ciliary mechanosensation and is activated in polycystic kidney disease. Dev Cell. 2006;10:57–69. doi: 10.1016/j.devcel.2005.12.005
72. Yao Q, Outeda P, Xu H, Walker R, Basquin D, Qian F, Cebotaru L, Watnick T, Cebotaru V. Polycystin-1 dependent regulation of polycystin-2 via GRP94, a member of HSP90 family that resides in the endoplasmic reticulum. Faseb j. 2021;35:e21865. doi: 10.1096/fj.202100325RR
73. Tesz GJ, Guilherme A, Guntur KV, Hubbard AC, Tang X, Chawla A, Czech MP. Tumor necrosis factor alpha (TNFalpha) stimulates Map4k4 expression through TNFalpha receptor 1 signaling to c-Jun and activating transcription factor 2. J Biol Chem. 2007;282:19302–19312. doi: 10.1074/jbc.M700665200
74. Chen K, Feng L, Hu W, Chen J, Wang X, Wang L, He Y. Optineurin inhibits NLRP3 inflammasome activation by enhancing mitophagy of renal tubular cells in diabetic nephropathy. Faseb j. 2019;33:4571–4585. doi: 10.1096/fj.201801749RRR
75. Chen K, Dai H, Yuan J, Chen J, Lin L, Zhang W, Wang L, Zhang J, Li K, He Y. Optineurin-mediated mitophagy protects renal tubular epithelial cells against accelerated senescence in diabetic nephropathy. Cell Death Dis. 2018;9:105. doi: 10.1038/s41419-017-0127-z
76. Nauta AJ, de Haij S, Bottazzi B, Mantovani A, Borrias MC, Aten J, Rastaldi MP, Daha MR, van Kooten C, Roos A. Human renal epithelial cells produce the long pentraxin PTX3. Kidney Int. 2005;67:543–553. doi: 10.1111/j.1523-1755.2005.67111.x
77. Tong M, Carrero JJ, Qureshi AR, Anderstam B, Heimbürger O, Bárány P, Axelsson J, Alvestrand A, Stenvinkel P, Lindholm B, et al. Plasma pentraxin 3 in patients with chronic kidney disease: associations with renal function, protein-energy wasting, cardiovascular disease, and mortality. Clin J Am Soc Nephrol. 2007;2:889–897. doi: 10.2215/cjn.00870207

# Figures

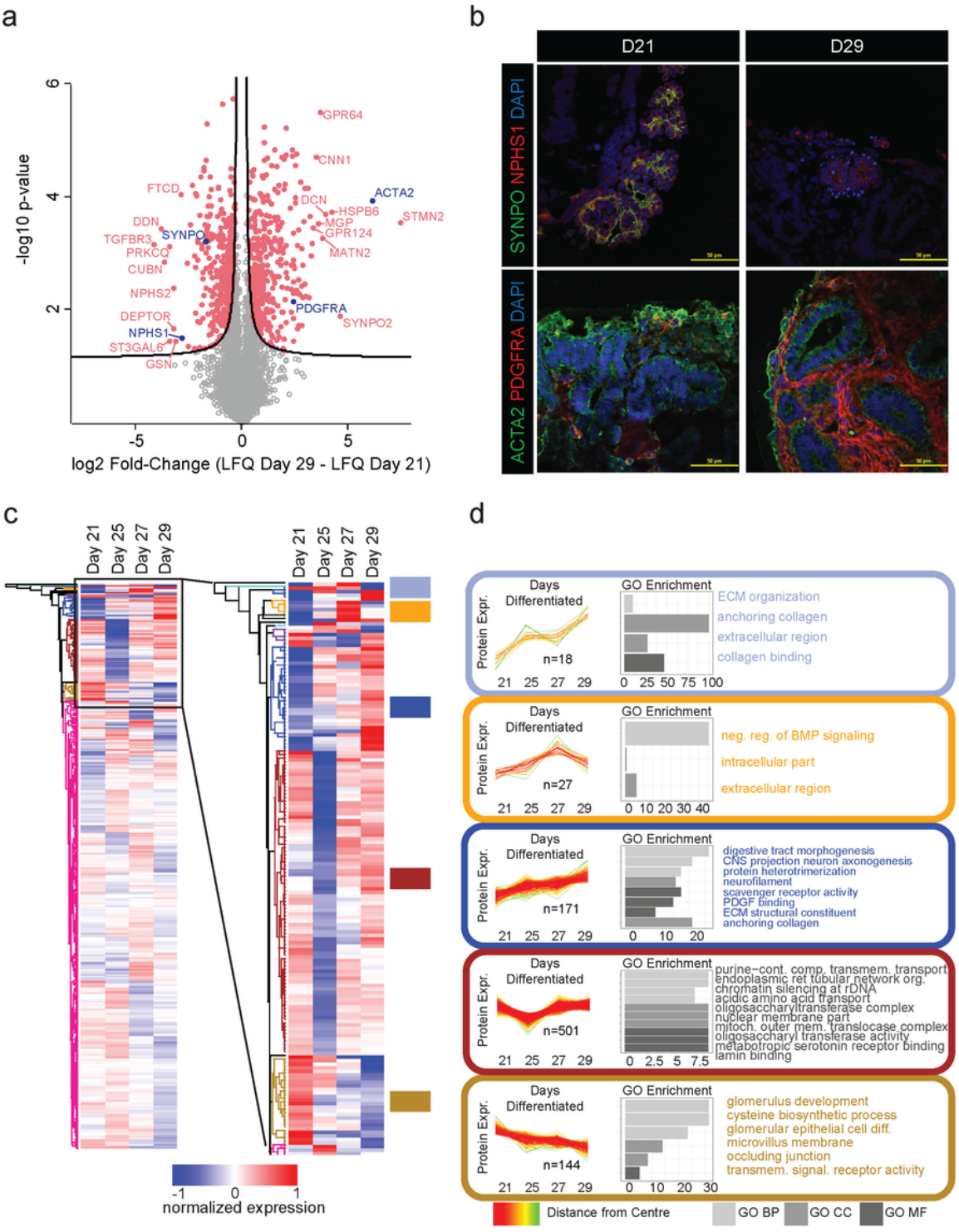


## Figure 1

Figure legend not available with this version.

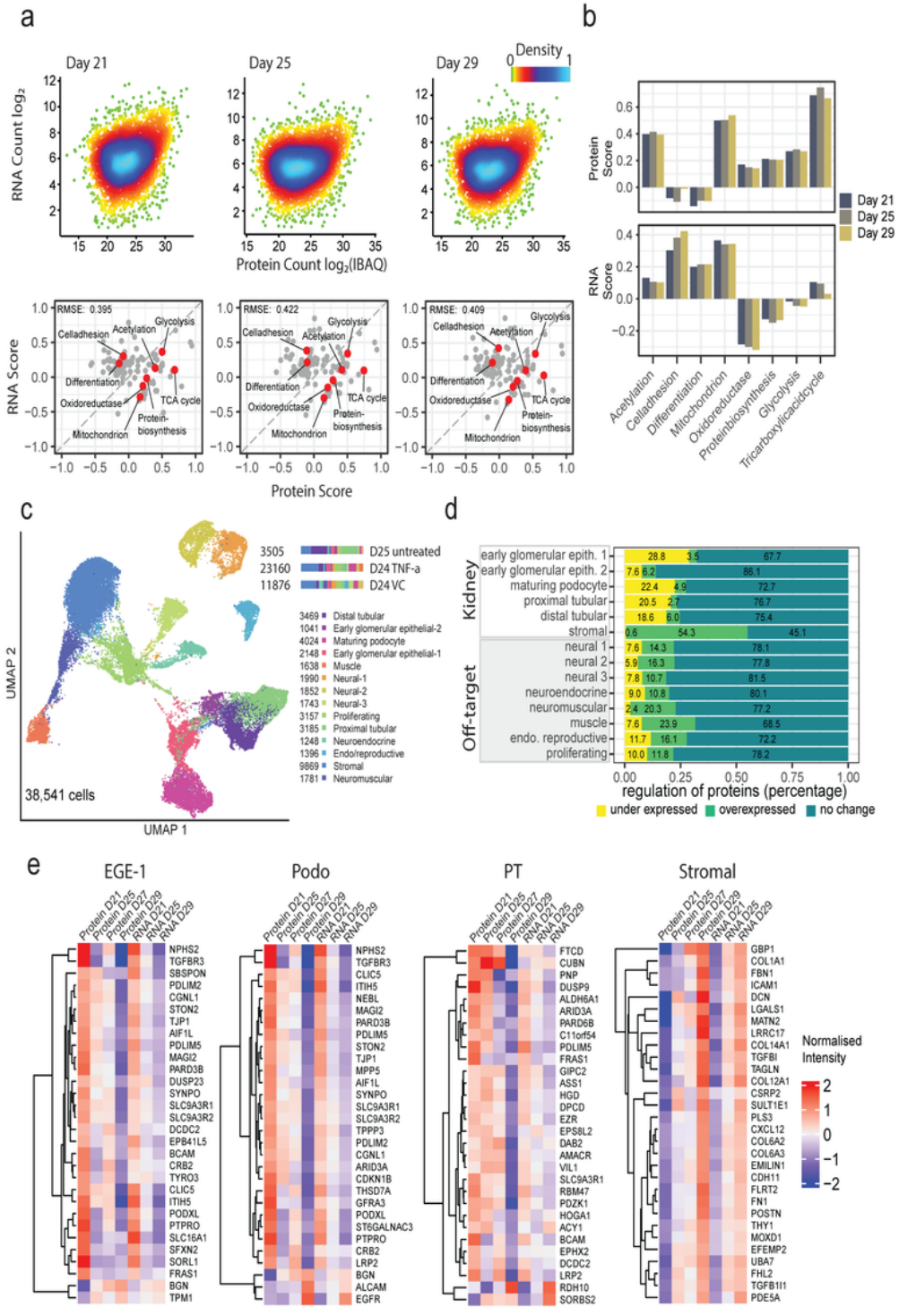


## Figure 2

Figure legend not available with this version.

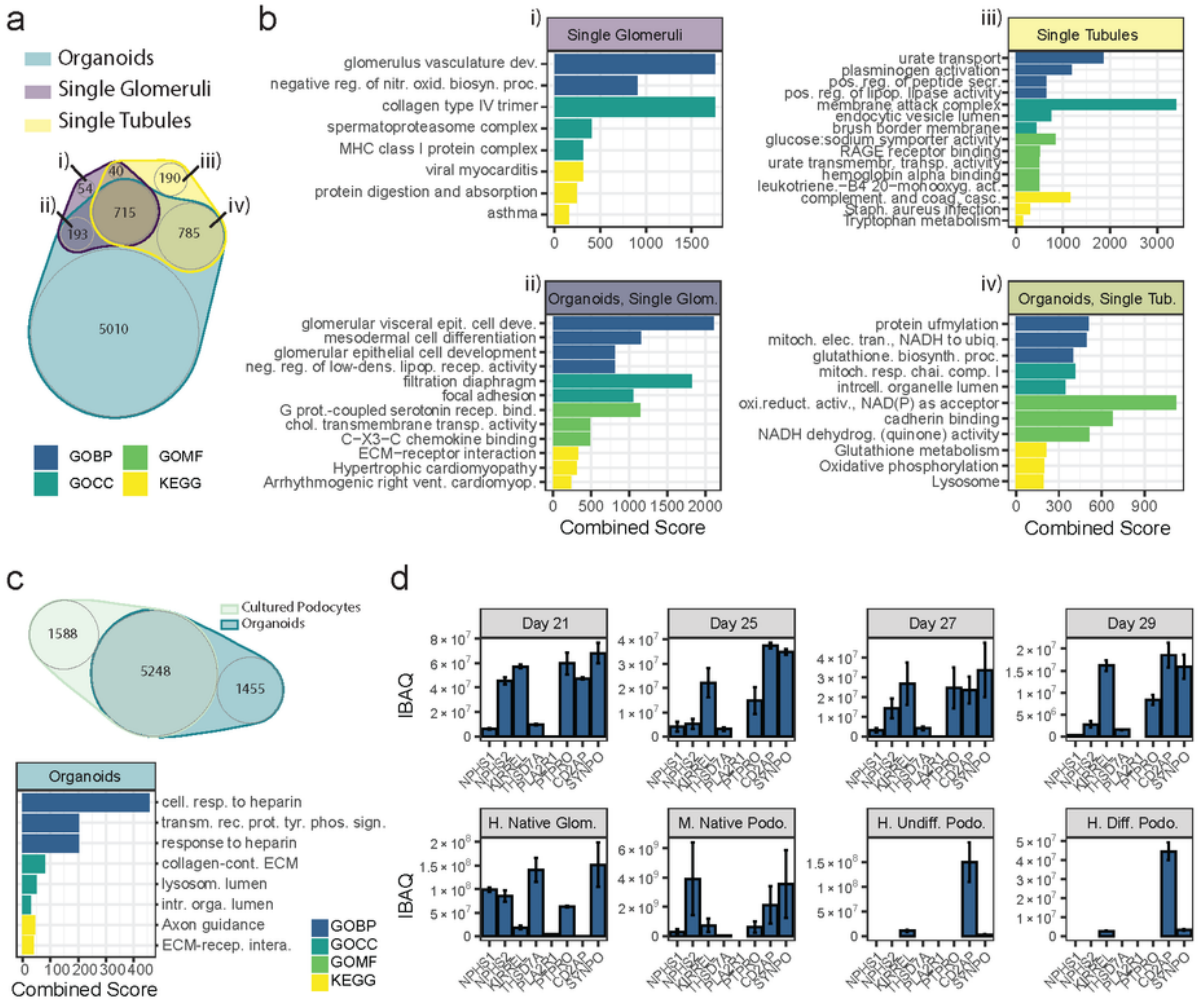


## Figure 3

Figure legend not available with this version.

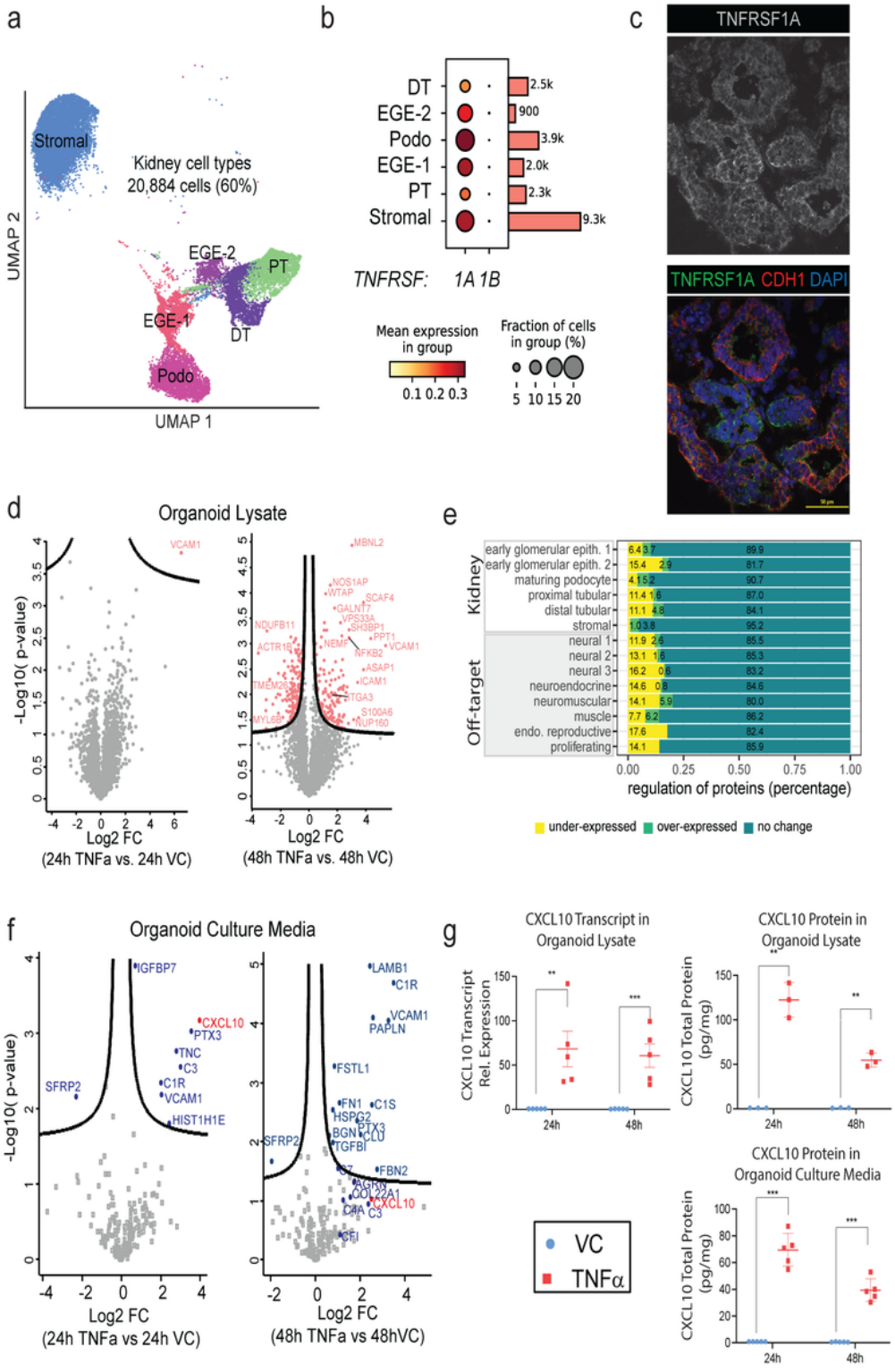


## Figure 4

Figure legend not available with this version.

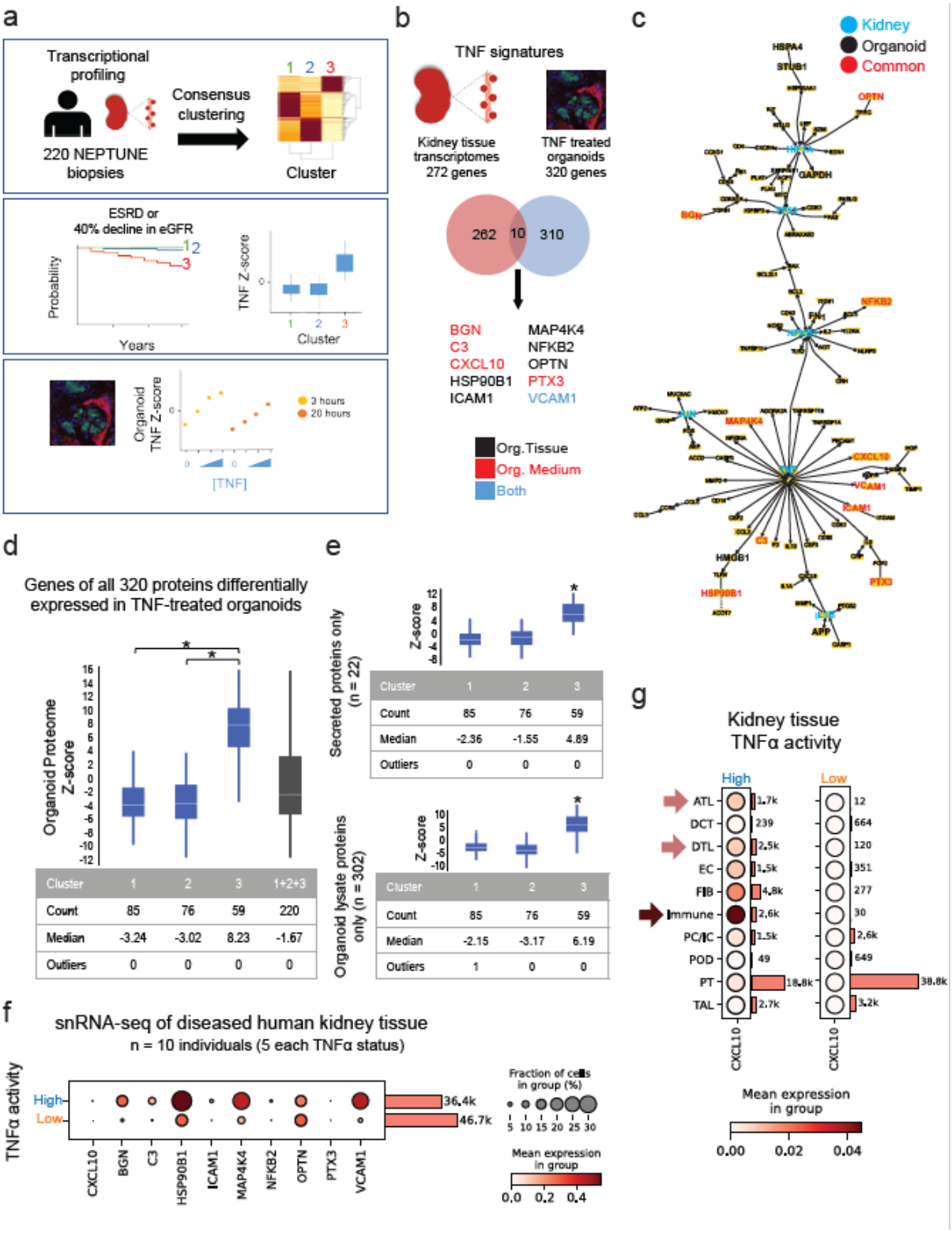


## Figure 5

Figure legend not available with this version.

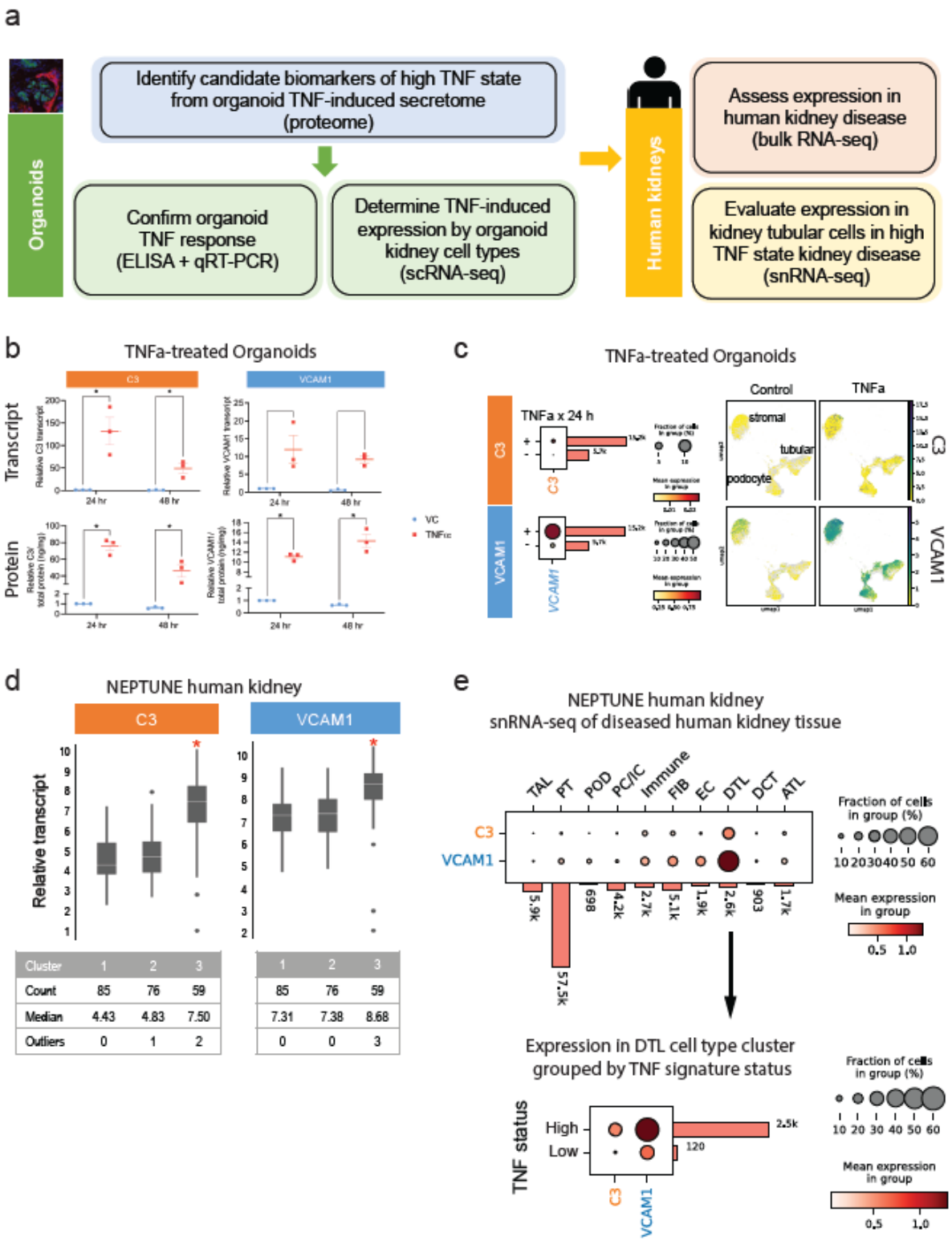


## Figure 6

Figure legend not available with this version.

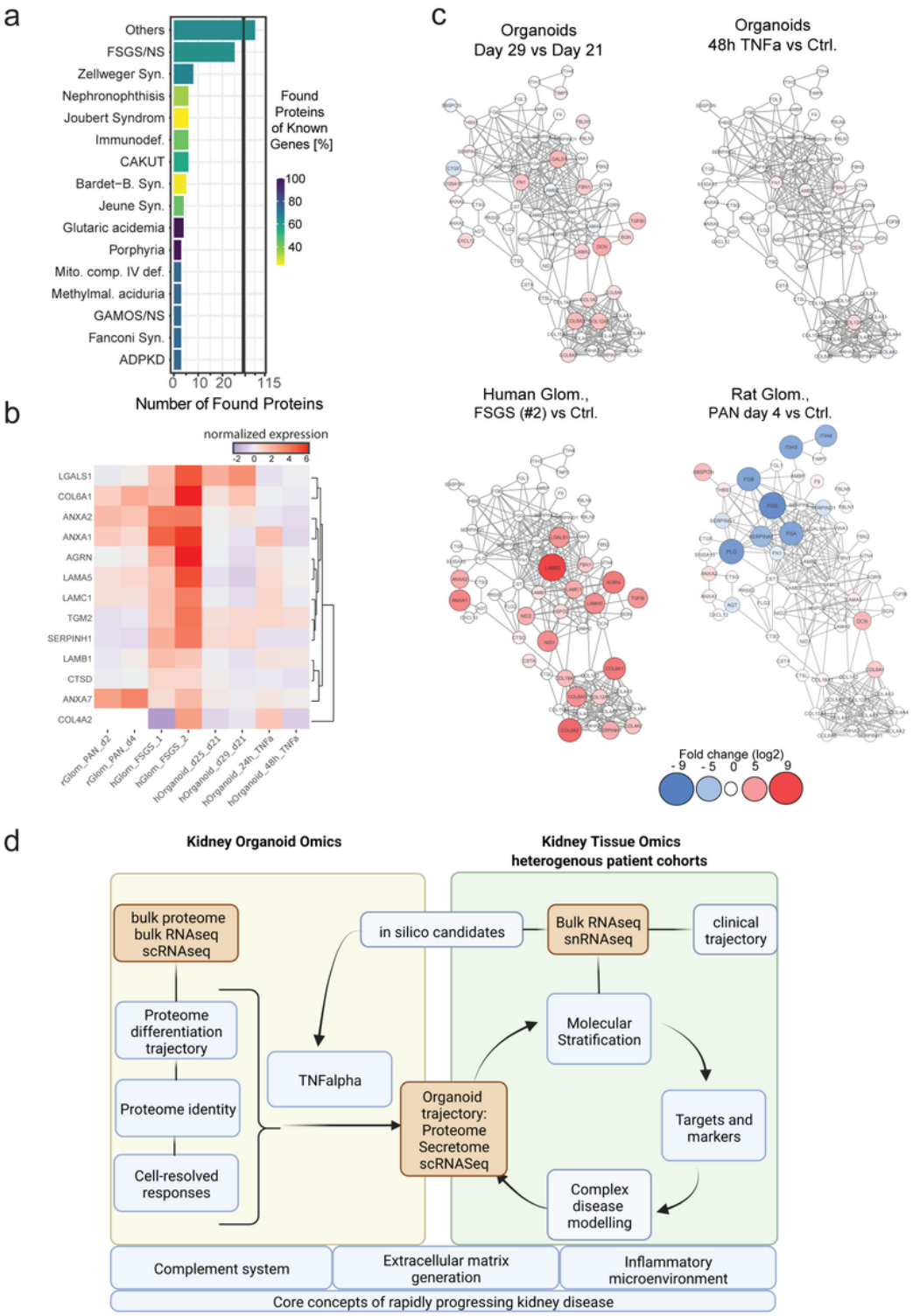


**Figure 7**

Figure legend not available with this version.

# Supplementary Files

This is a list of supplementary files associated with this preprint. Click to download.

- 20220927supptablesnatcomm.xlsx
- 20220927figuresnatcomm.pdf